

A QUANTITATIVE DESCRIPTION OF MEMBRANE CURRENT AND ITS APPLICATION TO CONDUCTION AND EXCITATION IN NERVE*

■ A. L. HODGKIN and A. F. HUXLEY
 Physiological Laboratory,
 University of Cambridge,
 Cambridge, U.K.

This article concludes a series of papers concerned with the flow of electric current through the surface membrane of a giant nerve fibre (Hodgkin *et al.*, 1952, *J. Physiol.* **116**, 424–448; Hodgkin and Huxley, 1952, *J. Physiol.* **116**, 449–566). Its general object is to discuss the results of the preceding papers (Section 1), to put them into mathematical form (Section 2) and to show that they will account for conduction and excitation in quantitative terms (Sections 3–6).

1. Discussion of Experimental Results. The results described in the preceding papers suggest that the electrical behaviour of the membrane may be represented by the network shown in Fig. 1. Current can be carried through the

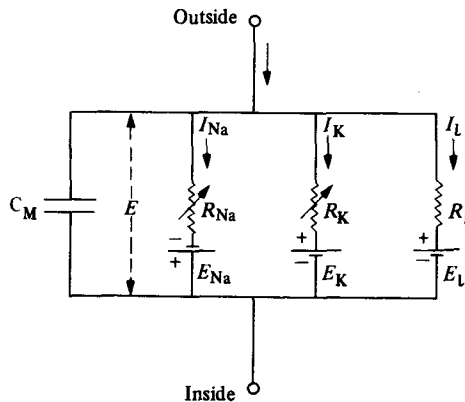


Figure 1. Electrical circuit representing membrane. $R_{Na} = 1/g_{Na}$; $R_K = 1/g_K$; $R_L = 1/g_L$. R_{Na} and R_K vary with time and membrane potential; the other components are constant.

membrane either by charging the membrane capacity or by movement of ions through the resistances in parallel with the capacity. The ionic current is divided into components carried by sodium and potassium ions (I_{Na} and I_K), and a small “leakage current” (I_L) made up by chloride and other ions. Each

* Reprinted from the *Journal of Physiology*, Vol. 117, pp. 500–544 (1952) with the permission of the Physiological Society.

component of the ionic current is determined by a driving force which may conveniently be measured as an electrical potential difference and a permeability coefficient which has the dimensions of a conductance. Thus the sodium current (I_{Na}) is equal to the sodium conductance (g_{Na}) multiplied by the difference between the membrane potential (E) and the equilibrium potential for the sodium ion (E_{Na}). Similar equations apply to I_{K} and I_{l} and are collected on p. 30 (p. 505 of original paper).

Our experiments suggest that g_{Na} and g_{K} are functions of time and membrane potential, but that E_{Na} , E_{K} , E_{l} , C_{M} and \bar{g}_{l} may be taken as constant. The influence of membrane potential on permeability can be summarized by stating: first, that depolarization causes a transient increase in sodium conductance and a slower but maintained increase in potassium conductance; secondly, that these changes are graded and that they can be reversed by repolarizing the membrane. In order to decide whether these effects are sufficient to account for complicated phenomena such as the action potential and refractory period, it is necessary to obtain expressions relating the sodium and potassium conductances to time and membrane potential. Before attempting this we shall consider briefly what types of physical system are likely to be consistent with the observed changes in permeability.

1.1. The nature of the permeability changes. At present the thickness and composition of the excitable membrane are unknown. Our experiments are therefore unlikely to give any certain information about the nature of the molecular events underlying changes in permeability. The object of this section is to show that certain types of theory are excluded by our experiments and that others are consistent with them.

The first point which emerges is that the changes in permeability appear to depend on membrane potential and not on membrane current. At a fixed depolarization the sodium current follows a time course whose form is independent of the current through the membrane. If the sodium concentration is such that $E_{\text{Na}} < E$, the sodium current is inward; if it is reduced until $E_{\text{Na}} > E$ the current changes in sign but still appears to follow the same time course. Further support for the view that membrane potential is the variable controlling permeability is provided by the observation that restoration of the normal membrane potential causes the sodium or potassium conductance to decline to a low value at any stage of the response.

The dependence of g_{Na} and g_{K} on membrane potential suggests that the permeability changes arise from the effect of the electric field on the distribution or orientation of molecules with a charge or dipole moment. By this we do not mean to exclude chemical reactions, for the rate at which these occur might depend on the position of a charged substrate or catalyst. All that is intended is that small changes in membrane potential would be most unlikely to cause

large alterations in the state of a membrane which was composed entirely of electrically neutral molecules.

The next question to consider is how changes in the distribution of a charged particle might affect the ease with which sodium ions cross the membrane. Here we can do little more than reject a suggestion which formed the original basis of our experiments (Hodgkin *et al.*, 1949). According to this view, sodium ions do not cross the membrane in ionic form but in combination with a lipid soluble carrier which bears a large negative charge and which can combine with one sodium ion but no more. Since both combined and uncombined carrier molecules bear a negative charge they are attracted to the outside of the membrane in the resting state. Depolarization allows the carrier molecules to move, so that sodium current increases as the membrane potential is reduced. The steady-state relation between sodium current and voltage could be calculated for this system and was found to agree reasonably with the observed curve at 0.2 ms after the onset of a sudden depolarization. This was encouraging, but the analogy breaks down if it is pursued further. In the model the first effect of depolarization is a movement of negatively charged molecules from the outside to the inside of the membrane. This gives an initial outward current, and an inward current does not occur until combined carriers lose sodium to the internal solution and return to the outside of the membrane. In our original treatment the initial outward current was reduced to vanishingly small proportions by assuming a low density of carriers and a high rate of movement and combination. Since we now know that the sodium current takes an appreciable time to reach its maximum, it is necessary to suppose that there are more carriers and that they react or move more slowly. This means that any inward current should be preceded by a large outward current. Our experiments show no sign of a component large enough to be consistent with the model. This invalidates the detailed mechanism assumed for the permeability change but it does not exclude the more general possibility that sodium ions cross the membrane in combination with a lipid soluble carrier.

A different form of hypothesis is to suppose that sodium movement depends on the distribution of charged particles which do not act as carriers in the usual sense, but which allow sodium to pass through the membrane when they occupy particular sites in the membrane. On this view the rate of movement of the activating particles determines the rate at which the sodium conductance approaches its maximum but has little effect on the magnitude of the conductance. It is therefore reasonable to find that temperature has a large effect on the rate of rise of sodium conductance but a relatively small effect on its maximum value. In terms of this hypothesis one might explain the transient nature of the rise in sodium conductance by supposing that the activating particles undergo a chemical change after moving from the position which they occupy when the membrane potential is high. An alternative is to attribute the

decline of sodium conductance to the relatively slow movement of another particle which blocks the flow of sodium ions when it reaches a certain position in the membrane.

Much of what has been said about the changes in sodium permeability applies equally to the mechanism underlying the change in potassium permeability. In this case one might suppose that there is a completely separate system which differs from the sodium system in the following respects: (1) the activating molecules have an affinity for potassium but not for sodium; (2) they move more slowly; (3) they are not blocked or inactivated. An alternative hypothesis is that only one system is present but that its selectivity changes soon after the membrane is depolarized. A situation of this kind would arise if inactivation of the particles selective for sodium converted them into particles selective for potassium. However, this hypothesis cannot be applied in a simple form since the potassium conductance rises too slowly for a direct conversion from a state of sodium permeability to one of potassium permeability.

One of the most striking properties of the membrane is the extreme steepness of the relation between ionic conductance and membrane potential. Thus g_{Na} may be increased e -fold by a reduction of only 4 mV, while the corresponding figure for g_{K} is 5–6 mV (Hodgkin and Huxley, 1952a, Figs 9 and 10). In order to illustrate the possible meaning of this result we shall suppose that a charged molecule which has some special affinity for sodium may rest either on the inside or the outside of the membrane but is present in negligible concentrations elsewhere. We shall also suppose that the sodium conductance is proportional to the number of such molecules on the inside of the membrane but is independent of the number on the outside. From Boltzmann's principle the proportion P_i of the molecules on the inside of the membrane is related to the proportion on the outside, P_o , by:

$$\frac{P_i}{P_o} = \exp[(w + zeE)/kT],$$

where E is the potential difference between the outside and the inside of the membrane, w is the work required to move the molecule from the inside to the outside of the membrane when $E=0$, e is the absolute value of the electronic charge z is the valency of the molecule (i.e. the number of positive electronic charges on it), k is Boltzmann's constant and T is the absolute temperature. Since we have assumed that $P_i + P_o = 1$ the expression for P_i is:

$$P_i = 1 / \left[1 + \exp\left(-\frac{w + zeE}{kT}\right) \right].$$

For negative values of z and with E sufficiently large and positive this gives:

$$P_i = \text{constant} \times \exp[zeE/kT].$$

In order to explain our results z must be about -6 since $kT/e (= RT/F)$ is 25 mV at room temperature and $g_{\text{Na}} \propto \exp -E/4$ for E large. This suggests that the particle whose distribution changes must bear six negative electronic charges, or, if a similar theory is developed in terms of the orientation of a long molecule with a dipole moment, it must have at least three negative charges on one end and three positive charges on the other. A different but related approach is to suppose that sodium movement depends on the presence of six singly charged molecules at a particular site near the inside of the membrane. The proportion of the time that each of the charged molecules spends at the inside is determined by $\exp -E/25$ so that the proportion of sites at which all six are at the inside is $\exp -E/4.17$. This suggestion may be given plausibility but not mathematical simplicity by imagining that a number of charges form a bridge or chain which allows sodium ions to flow through the membrane when it is depolarized. Details of the mechanism will probably not be settled for some time, but it seems difficult to escape the conclusion that the changes in ionic permeability depend on the movement of some component of the membrane which behaves as though it had a large charge or dipole moment. If such components exist it is necessary to suppose that their density is relatively low and that a number of sodium ions cross the membrane at a single active patch. Unless this were true one would expect the increase in sodium permeability to be accompanied by an outward current comparable in magnitude to the current carried by sodium ions. For movement of any charged particle in the membrane should contribute to the total current and the effect would be particularly marked with a molecule, or aggregate, bearing a large charge. As was mentioned earlier, there is no evidence from our experiments of any current associated with the change in sodium permeability, apart from the contribution of the sodium ion itself. We cannot set a definite upper limit to this hypothetical current, but it could hardly have been more than a few per cent of the maximum sodium current without producing a conspicuous effect at the sodium potential.

2. Mathematical Description of Membrane Current During a Voltage Clamp

2.1. Total membrane current. The first step in our analysis is to divide the total membrane current into a capacity current and an ionic current. Thus:

$$I = C_M \frac{dV}{dt} + I_i, \quad (1)$$

where: I is the total membrane current density (inward current positive); I_i is the ionic current density (inward current positive); V is the displacement of the membrane potential from its resting value (depolarization negative); C_M is the membrane capacity per unit area (assumed constant); t is time.

The justification for this equation is that it is the simplest which can be used and that it gives values for the membrane capacity which are independent of the magnitude or sign of V and are little affected by the time course of V (see, for example, Table 1 of Hodgkin *et al.*, 1952). Evidence that the capacity current and ionic current are in parallel [as suggested by equation (1)] is provided by the similarity between ionic currents measured with $dV/dt=0$ and those calculated from $-C_M(dV/dt)$ with $I=0$ (Hodgkin *et al.*, 1952).

The only major reservation which must be made about equation (1) is that it takes no account of dielectric loss in the membrane. There is no simple way of estimating the error introduced by this approximation, but it is not thought to be large since the time course of the capacitative surge was reasonably close to that calculated for a perfect condenser (Hodgkin *et al.*, 1952).

2.1.1. The ionic current. A further sub-division of the membrane current can be made by splitting the ionic current into components carried by sodium ions (I_{Na}), potassium ions (I_K) and other ions (I_1):

$$I_i = I_{Na} + I_K + I_1. \quad (2)$$

2.1.2. The individual ionic currents. In the second paper of this series (Hodgkin and Huxley, 1952b) we showed that the ionic permeability of the membrane could be satisfactorily expressed in terms of ionic conductances (g_{Na} , g_K and \bar{g}_1). The individual ionic currents are obtained from these by the relations:

$$I_{Na} = g_{Na}(E - E_{Na}),$$

$$I_K = g_K(E - E_K),$$

$$I_1 = \bar{g}_1(E - E_1),$$

where E_{Na} and E_K are the equilibrium potentials for the sodium and potassium ions. E_1 is the potential at which the "leakage current" due to chloride and other ions is zero. For practical application it is convenient to write these equations in the form:

$$I_{Na} = g_{Na}(V - V_{Na}), \quad (3)$$

$$I_K = g_K(V - V_K), \quad (4)$$

$$I_1 = \bar{g}_1(V - V_1), \quad (5)$$

where:

$$\begin{aligned} V &= E - E_r, \\ V_{\text{Na}} &= E_{\text{Na}} - E_r, \\ V_{\text{K}} &= E_{\text{K}} - E_r, \\ V_{\text{I}} &= E_{\text{I}} - E_r, \end{aligned}$$

and E_r is the absolute value of the resting potential. V , V_{Na} , V_{K} and V_{I} can then be measured directly as displacements from the resting potential.

2.2. The ionic conductances. The discussion in Section 1 shows that there is little hope of calculating the time course of the sodium and potassium conductances from first principles. Our object here is to find equations which describe the conductances with reasonable accuracy and are sufficiently simple for theoretical calculation of the action potential and refractory period. For the sake of illustration we shall try to provide a physical basis for the equations, but must emphasize that the interpretation given is unlikely to provide a correct picture of the membrane.

At the outset there is the difficulty that both sodium and potassium conductances increase with a delay when the axon is depolarized but fall with no appreciable inflexion when it is repolarized. This is illustrated by the circles in Fig. 2, which shows the change in potassium conductance associated with a

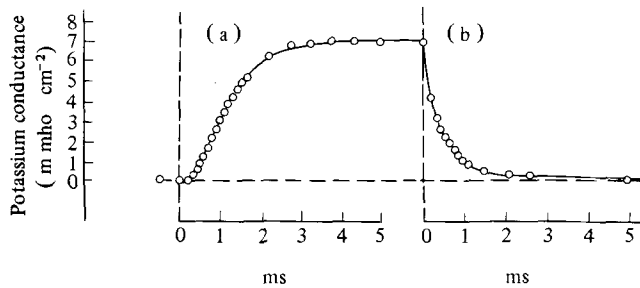


Figure 2. (a) Rise of potassium conductance associated with depolarization of 25 mV; (b) fall of potassium conductance associated with repolarization to the resting potential. Circles: experimental points replotted from Hodgkin and Huxley (1952b, Fig. 13). The last point of (a) is the same as the first point in (b). Axon 18, 21°C in choline sea water. The smooth curve is drawn according to equation (11) with the following parameters.

	Curve (a) ($V = -25$ mV)	Curve (b) ($V = 0$)
$g_{\text{K}0}$	0.09 m mho cm^{-2}	7.06 m mho cm^{-2}
$g_{\text{K}\infty}$	7.06 m mho cm^{-2}	0.09 m mho cm^{-2}
τ_n	0.75 ms	1.1 ms

depolarization of 25 mV lasting 4.9 ms. If g_K is used as a variable the end of the record can be fitted by a first-order equation but a third- or fourth-order equation is needed to describe the beginning. A useful simplification is achieved by supposing that g_K is proportional to the fourth power of a variable which obeys a first-order equation. In this case the rise of potassium conductance from zero to a finite value is described by $(1 - \exp(-t))^4$, while the fall is given by $\exp(-4t)$. The rise in conductance therefore shows a marked inflexion, while the fall is a simple exponential. A similar assumption using a cube instead of a fourth power describes the initial rise of sodium conductance, but a term representing inactivation must be included to cover the behaviour at long times.

2.2.1. The potassium conductance. The formal assumptions used to describe the potassium conductance are:

$$g_K = \bar{g}_K n^4, \quad (6)$$

$$\frac{dn}{dt} = \alpha_n(1 - n) - \beta_n n, \quad (7)$$

where \bar{g}_K is a constant with the dimensions of conductance per cm^2 , α_n and β_n are rate constants which vary with voltage but not with time and have dimensions of $[\text{time}]^{-1}$, n is a dimensionless variable which can vary between 0 and 1.

These equations may be given a physical basis if we assume that potassium ions can only cross the membrane when four similar particles occupy a certain region of the membrane: n represents the proportion of the particles in a certain position (for example at the inside of the membrane) and $1 - n$ represents the proportion that are somewhere else (for example at the outside of the membrane); α_n determines the rate of transfer from outside to inside, while β_n determines the transfer in the opposite direction. If the particle has a negative charge α_n should increase and β_n should decrease when the membrane is depolarized.

Application of these equations will be discussed in terms of the family of curves in Fig. 3. Here the circles are experimental observations of the rise of potassium conductance associated with depolarization, while the smooth curves are theoretical solutions of equations (6) and (7).

In the resting state, defined by $\Gamma = 0$, n has a resting value given by:

$$n_0 = \frac{\alpha_{n0}}{\alpha_{n0} + \beta_{n0}}.$$

If V is changed suddenly α_n and β_n instantly take up values appropriate to the

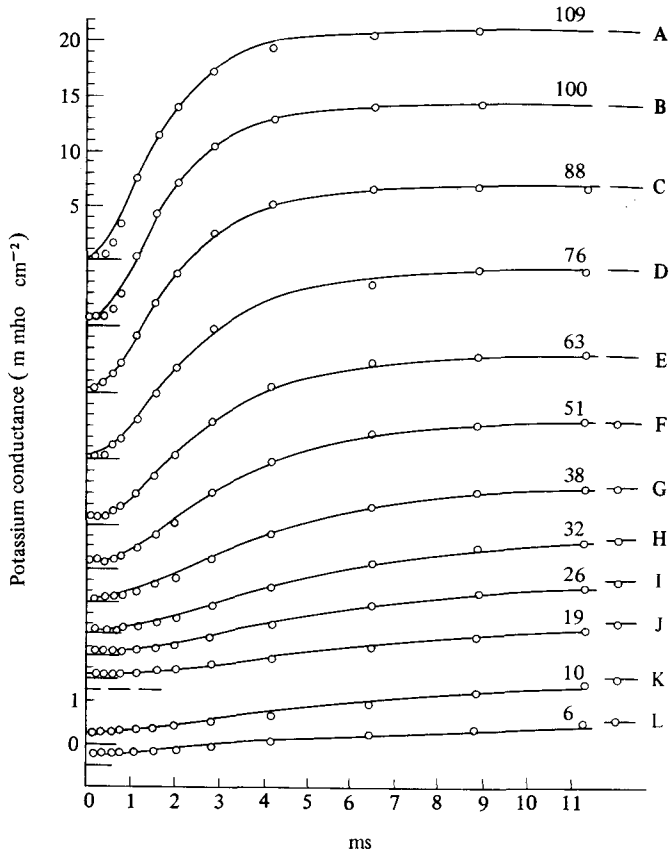


Figure 3. Rise of potassium conductance associated with different depolarizations. The circles are experimental points obtained on axon 17, temperature 6–7°C, using observations in sea water and choline sea water (see Hodgkin and Huxley, 1952a). The smooth curves were drawn from equation (11) with $g_{K0} = 0.24$ m mho cm^{-2} and other parameters as shown in Table 1. The time scale applies to all records. The ordinate scale is the same in the upper 10 curves (A–J) and is increased four-fold in the lower two curves (K and L). The number on each curve gives the depolarization in mV.

new voltage. The solution of equation (7) which satisfies the boundary condition that $n = n_0$ when $t = 0$ is:

$$n = n_{\infty} - (n_{\infty} - n_0)\exp(-t/\tau_n), \quad (8)$$

where:

$$n_{\infty} = \alpha_n / (\alpha_n + \beta_n), \quad (9)$$

and:

$$\tau_n = 1/(\alpha_n + \beta_n). \quad (10)$$

From equation (6) this may be transformed into a form suitable for comparison with the experimental results, i.e.

$$g_K = \{(g_{K\infty})^{1/4} - [(g_{K\infty})^{1/4} - (g_{K0})^{1/4}] \exp(-t/\tau_n)\}^4, \quad (11)$$

where $g_{K\infty}$ is the value which the conductance finally attains and g_{K0} is the conductance at $t=0$. The smooth curves in Fig. 3 were calculated from equation (11) with a value of τ_n chosen to give the best fit. It will be seen that there is reasonable agreement between theoretical and experimental curves, except that the latter show more initial delay. Better agreement might have been obtained with a fifth or sixth power, but the improvement was not considered to be worth the additional complication.

The rate constants α_n and β_n . At large depolarizations $g_{K\infty}$ seems to approach an asymptote about 20–50% greater than the conductance at -100 mV.

For the purpose of calculation we assume that $n=1$ at the asymptote which is taken as about 20% greater than the value of $g_{K\infty}$ at $V = -100$ mV. These assumptions are somewhat arbitrary, but should introduce little error since we are not concerned with the behaviour of g_K at depolarizations greater than about 110 mV. In the experiment illustrated by Fig. 3, $g_{K\infty} = 20$ m mho cm^{-2} at $V = -100$ mV; \bar{g}_K was therefore chosen to be near 24 m mho cm^{-2} . This value was used to calculate n_∞ at various voltages by means of equation (6). α_n and β_n could then be obtained from the following relations which are derived from equations (9) and (10):

$$\begin{aligned} \alpha_n &= n_\infty/\tau_n, \\ \beta_n &= (1 - n_\infty)/\tau_n. \end{aligned}$$

The results of analysing the curves in Fig. 3 by this method are shown in Table 1.

An estimate of the resting values of α_n and β_n could be obtained from the decline in potassium conductance associated with repolarization. The procedure was essentially the same but the results were approximate because the resting value of the potassium conductance was not known with any accuracy when the membrane potential was high. Figure 2 illustrates an experiment in which the membrane potential was restored to its resting value after a depolarization of 25 mV. It will be seen that both the rise and fall of the potassium conductance agree reasonably with theoretical curves calculated from equation (11) after an appropriate choice of parameters. The rate constants derived from these parameters were (ms^{-1}): $\alpha_n = 0.21$, $\beta_n = 0.70$ when $V=0$ and $\alpha_n = 0.90$, $\beta_n = 0.43$ when $V = -25$ mV.

Table 1. Analysis of Curves in Fig. 3

Curve	V (mV)	$g_{K\infty}$ (m mho cm ⁻²)	n_{∞}	τ_n (ms)	α_n (m s ⁻¹)	β_n (m s ⁻¹)
—	($-\infty$)	(24.31)	(1.000)	—	—	—
A	-109	20.70	0.961	1.05	0.915	0.037
B	-100	20.00	0.953	1.10	0.866	0.043
C	-88	18.60	0.935	1.25	0.748	0.052
D	-76	17.00	0.915	1.50	0.610	0.057
E	-63	15.30	0.891	1.70	0.524	0.064
F	-51	13.27	0.859	2.05	0.419	0.069
G	-38	10.29	0.806	2.60	0.310	0.075
H	-32	8.62	0.772	3.20	0.241	0.071
I	-26	6.84	0.728	3.80	0.192	0.072
J	-19	5.00	0.674	4.50	0.150	0.072
K	-10	1.47	0.496	5.25	0.095	0.096
L	-6	0.98	0.448	5.25	0.085	0.105
—	(0)	(0.24)	(0.315)	—	—	—

The figure of 24.31 was chosen for \bar{g}_K because it made the asymptotic value of n_{∞} 5% greater than the value at -100 mV.

In order to find functions connecting α_n and β_n with membrane potential we collected all our measurements and plotted them against V , as in Fig. 4. Differences in temperature were allowed for by adopting a temperature coefficient of three (Hodgkin *et al.*, 1952) and scaling to 6°C. The effect of replacing sodium by choline on the resting potential was taken into account by displacing the origin for values in choline sea water by $+4$ mV. The continuous curves, which are clearly a good fit to the experimental data, were calculated from the following expressions:

$$\alpha_n = 0.01(V + 10) / \left[\exp \frac{V + 10}{10} - 1 \right], \quad (12)$$

$$\beta_n = 0.125 \exp(V/80), \quad (13)$$

where α_n and β_n are given in reciprocal msec and V is the displacement of the membrane potential from its resting value in mV.

These expressions should also give a satisfactory formula for the steady potassium conductance ($g_{K\infty}$) at any membrane potential (V), for this relation is implicit in the measurement of α_n and β_n . This is illustrated by Fig. 5, in which the abscissa is the membrane potential and the ordinate is $(g_{K\infty}/\bar{g}_K)^{1/4}$. The smooth curve was calculated from equation (9) with α_n and β_n substituted from equations (12) and (13).

Figure 4 shows that β_n is small compared to α_n over most of the range; we

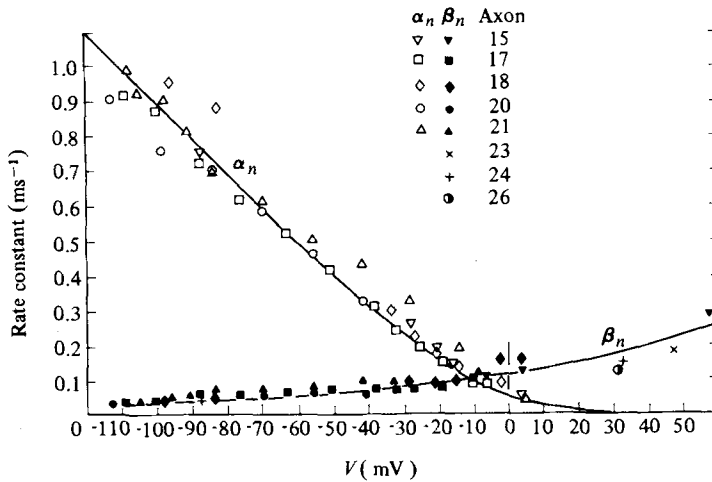


Figure 4. Abscissa: membrane potential minus resting potential in sea water. Ordinate: rate constants determining rise (α_n) or fall (β_n) of potassium conductance at 6°C. The resting potential was assumed to be 4 mV higher in choline sea water than in ordinary sea water. Temperature differences were allowed for by assuming a Q_{10} of 3. All values for $V < 0$ were obtained by the method illustrated by Fig. 3 and Table 1; those for $V > 0$ were obtained from the decline of potassium conductance associated with an increase of membrane potential or from repolarization to the resting potential in choline sea water (e.g. Fig. 2). Axons 17-21 at 6-11°C, the remainder at about 20°C. The smooth curves were drawn from equations (12) and (13).

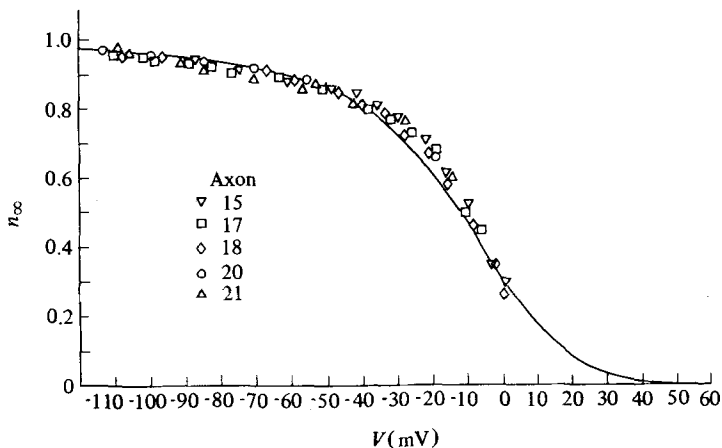


Figure 5. Abscissa: membrane potential minus resting potential in sea water. Ordinate: experimental measurements of n_∞ calculated from the steady potassium conductance by the relation $n_\infty = (g_{K\infty}/\bar{g}_K)^{1/4}$, where \bar{g}_K is the "membrane" potassium conductance. The smooth curve is drawn according to equation (9).

therefore do not attach much weight to the curve relating β_n to V and have used the simplest expression which gave a reasonable fit. The function for α_n was chosen for two reasons. First, it is one of the simplest which fits the experimental results and, secondly, it bears a close resemblance to the equation derived by Goldman (1943) for the movements of a charged particle in a constant field. Our equations can therefore be given a qualitative physical basis if it is supposed that the variation of α and β with membrane potential arises from the effect of the electric field on the movement of a negatively charged particle which rests on the outside of the membrane when V is large and positive, and on the inside when it is large and negative. The analogy cannot be pressed since α and β are not symmetrical about $E=0$, as they should be if Goldman's theory held in a simple form. Better agreement might be obtained by postulating some asymmetry in the structure of the membrane, but this assumption was regarded as too speculative for profitable consideration.

2.2.2. The sodium conductance. There are at least two general methods of describing the transient changes in sodium conductance. First, we might assume that the sodium conductance is determined by a variable which obeys a second-order differential equation. Secondly, we might suppose that it is determined by two variables, each of which obeys a first-order equation. These two alternatives correspond roughly to the two general types of mechanism mentioned in connection with the nature of inactivation (pp. 27–28; pp. 502–503 of original paper). The second alternative was chosen since it was simpler to apply to the experimental results.

The formal assumptions made are:

$$g_{\text{Na}} = m^3 h \bar{g}_{\text{Na}}, \quad (14)$$

$$\frac{dm}{dt} = \alpha_m(1-m) - \beta_m m, \quad (15)$$

$$\frac{dh}{dt} = \alpha_h(1-h) - \beta_h h, \quad (16)$$

where \bar{g}_{Na} is a constant and the α 's and β 's are functions of V but not of t .

These equations may be given a physical basis if sodium conductance is assumed to be proportional to the number of sites on the inside of the membrane which are occupied simultaneously by three activating molecules but are not blocked by an inactivating molecule. In which case, m represents the proportion of activating molecules on the inside and $1-m$ the proportion on the outside; h is the proportion of inactivating molecules on the outside and $1-h$ the proportion on the inside. α_m or β_h and β_m or α_h represent the transfer rate constants in the two directions.

Application of these equations will be discussed first in terms of the family of curves in Fig. 6. Here the circles are experimental estimates of the rise and fall of sodium conductance during a voltage clamp, while the smooth curves were calculated from equations (14)–(16).

The solutions of equations (15) and (16) which satisfy the boundary conditions $m = m_0$ and $h = h_0$ at $t = 0$ are:

$$m = m_\infty - (m_\infty - m_0)\exp(-t/\tau_m), \quad (17)$$

$$h = h_\infty - (h_\infty - h_0)\exp(-t/\tau_h), \quad (18)$$

where:

$$m_\infty = \alpha_m / (\alpha_m + \beta_m) \quad \text{and} \quad \tau_m = 1 / (\alpha_m + \beta_m),$$

$$h_\infty = \alpha_h / (\alpha_h + \beta_h) \quad \text{and} \quad \tau_h = 1 / (\alpha_h + \beta_h),$$

In the resting state the sodium conductance is very small compared with the value attained during a large depolarization. We therefore neglect m_0 if the depolarization is greater than 30 mV. Further, inactivation is very nearly complete if $V < -30$ mV so that h_∞ may also be neglected. The expression for the sodium conductance then becomes:

$$g_{\text{Na}} = g'_{\text{Na}} [1 - \exp(-t/\tau_m)]^3 \exp(-t/\tau_h), \quad (19)$$

where $g'_{\text{Na}} = \bar{g}_{\text{Na}} m_\infty^3 h_0$ and is the value which the sodium conductance would attain if h remained at its resting level (h_0). Equation (19) was fitted to an experimental curve by plotting the latter on double log paper and comparing it with a similar plot of a family of theoretical curves drawn with different ratios of τ_m to τ_h . Curves A–H in Fig. 6 were obtained by this method and gave the values of g'_{Na} , τ_m and τ_h shown in Table 2. Curves I–L were obtained from equations (17) and (18) assuming that h_∞ and τ_h had values calculated from experiments described in a previous paper (Hodgkin and Huxley, 1952c).

The rate constants α_m and β_m . Having fitted theoretical curves to the experimental points, α_m and β_m were found by a procedure similar to that used with α_n and β_n , i.e.

$$\alpha_m = m_\infty / \tau_m, \quad \beta_m = (1 - m_\infty) / \tau_m,$$

the value of m_∞ being obtained from $g'_{\text{Na}}^{1/3}$ on the basis that m_∞ approaches unity at large depolarizations.

Values of α_m and β_m were collected from different experiments, reduced to at temperature of 6°C by adopting a Q_{10} of 3 and plotted in the manner shown in Fig. 7. The point for $V = 0$ was obtained from what we regard as the most

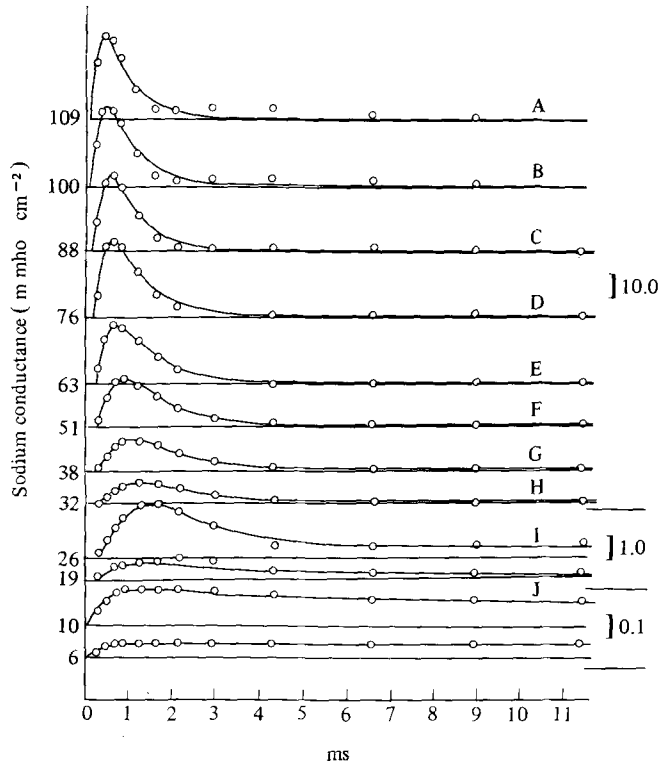


Figure 6. Changes of sodium conductance associated with different depolarizations. The circles are experimental estimates of sodium conductance obtained on axon 17, temperature 6–7°C (cf. Fig. 3). The smooth curves are theoretical curves with parameters shown in Table 2: A–H drawn from equation (19), I–L from 14, 17, 18 with $\bar{g}_{Na} = 70.7 \text{ m mho cm}^{-2}$. The ordinate scales on the right are given in m mho cm^{-2} . The numbers on the left show the depolarization in mV. The time scale applies to all curves.

reliable estimate of the rate constant determining the decline of sodium conductance when the membrane is repolarized (Hodgkin and Huxley, 1952b, Table 1, axon 41). The smooth curves in Fig. 7 were drawn according to the equations:

$$\alpha_m = 0.1(V+25) \left/ \left(\exp \frac{V+25}{10} - 1 \right) \right., \quad (20)$$

$$\beta_m = 4 \exp(V/18), \quad (21)$$

where α_m and β_m are expressed in ms^{-1} and V is in mV.

Figure 8 illustrates the relation between m_∞ and V . The symbols are

Table 2. Analysis of curves in Fig. 6

Curve	V (mV)	g_{Na}^0 (m mho cm ⁻²)	m_∞	τ_m (ms)	α_m (ms ⁻¹)	β_m (ms ⁻¹)	τ_h (ms)	h_∞	α_h (ms ⁻¹)	β_h (ms ⁻¹)
—	($-\infty$)	(42.9)	(1.00)	—	—	—	—	—	—	—
A	-109	40.3	0.980	0.140	7.0	(0.14)	0.67	(0)	(0)	1.50
B	-100	42.6	0.997	0.160	6.2	(0.02)	0.67	(0)	(0)	1.50
C	-88	46.8	1.029	0.200	5.15	(-0.14)	0.67	(0)	(0)	1.50
D	-76	39.5	0.975	0.189	5.15	0.13	0.84	(0)	(0)	1.19
E	-63	38.2	0.963	0.252	3.82	0.15	0.84	(0)	(0)	1.19
F	-51	30.7	0.895	0.318	2.82	0.33	1.06	(0)	(0)	0.94
G	-38	20.0	0.778	0.382	2.03	0.58	1.27	(0)	(0)	0.79
H	-32	15.3	0.709	0.520	1.36	0.56	1.33	(0)	(0)	0.75
I	-26	7.90	0.569	0.600	0.95	0.72	(1.50)	(0.029)	(0.02)	(0.65)
J	-19	1.44	0.323	0.400	0.81	1.69	(2.30)	(0.069)	(0.03)	(0.40)
K	-10	0.13	0.145	0.220	0.66	3.9	(5.52)	(0.263)	(0.05)	(0.13)
L	-6	0.046	0.103	0.200	0.51	4.5	(6.73)	(0.388)	(0.06)	(0.09)
—	(0)	(0.0033)	(0.042)	—	—	—	—	(0.608)	—	—

Values enclosed in brackets were not plotted in Figs 7-10 either because they were too small to be reliable or because they were not independent measurements obtained in this experiment.

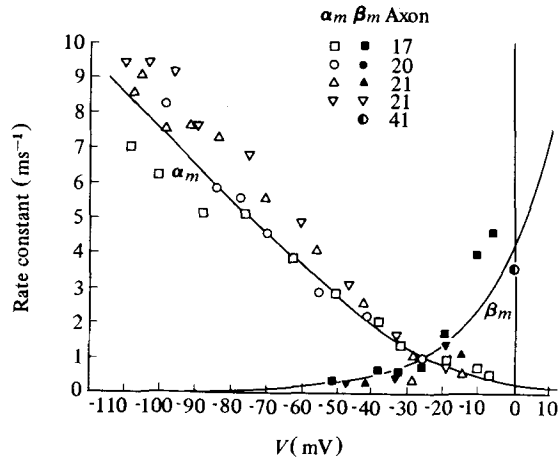


Figure 7. Abscissa: membrane potential minus resting potential in sea water. Ordinate: rate constants (α_m and β_m) determining initial changes in sodium conductance at 6°C. All values for $V < 0$ were obtained by the method illustrated by Fig. 6 and Table 2; the value at $V = 0$ was obtained from the decline in sodium conductance associated with repolarization to the resting potential. The temperature varied between 3 and 11°C and was allowed for by assuming a Q_{10} of 3. The smooth curves were drawn from equations (20) and (21).

experimental estimates and the smooth curve was calculated from the equation:

$$m_\infty = \alpha_m / (\alpha_m + \beta_m), \quad (22)$$

where α_m and β_m have the values given by equations (20) and (21).

The rate constants α_h and β_h . The rate constants for the inactivation process were calculated from the expressions:

$$\begin{aligned} \alpha_h &= h_\infty / \tau_h, \\ \beta_h &= (1 - h_\infty) / \tau_h. \end{aligned}$$

Values obtained by these equations are plotted against membrane potential in Fig. 9. The points for $V < -30$ mV were derived from the analysis described in this paper (e.g. Table 2), while those for $V > -30$ mV were obtained from the results given in a previous paper (Hodgkin and Huxley, 1952c). A temperature coefficient of 3 was assumed and differences in resting potential were allowed for by taking the origin at a potential corresponding to $h_\infty = 0.6$.

The smooth curves in this figure were calculated from the expressions:

$$\alpha_h = 0.07 \exp(V/20), \quad (23)$$

and:

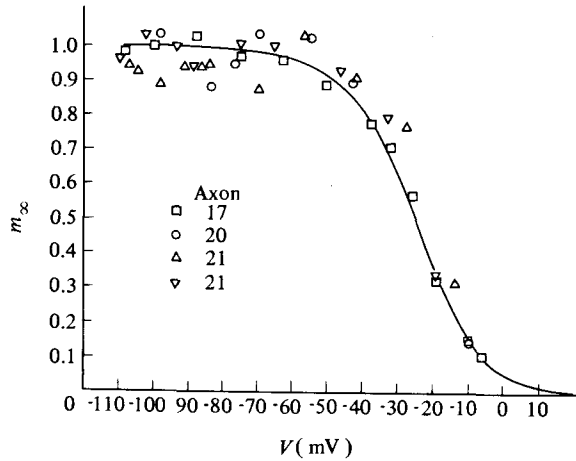


Figure 8. Abscissa: membrane potential minus resting potential in sea water. Ordinate: m_{∞} obtained by fitting curves to observed changes in sodium conductance at different depolarizations (e.g. Fig. 6 and Table 2). The smooth curve is drawn according to equation (22). The experimental points are proportional to the cube root of the sodium conductance which would have been obtained if there were no inactivation.

$$\beta_h = 1 / \left(\exp \frac{V+30}{10} + 1 \right). \quad (24)$$

The steady-state relation between h_{∞} and V is shown in Fig. 10. The smooth curve is calculated from the relation:

$$h_{\infty} = \alpha_h / (\alpha_h + \beta_h), \quad (25)$$

with α_h and β_h given by equations (23) and (24). If $V > -30$ mV this expression approximates to the simple expression used in a previous paper (Hodgkin and Huxley, 1952c), i.e.

$$h_{\infty} = 1 / \left(1 + \exp \frac{V_h - V}{7} \right),$$

where V_h is about -2 and is the potential at which $h_{\infty} = 0.5$. This equation is the same as that giving the effect of a potential difference on the proportion of negatively charged particles on the outside of a membrane to the total number of such particles on both sides of the membrane (see p. 28; p. 503 of original paper). It is therefore consistent with the suggestion that inactivation might be due to the movement of a negatively charged particle which blocks the flow of sodium ions when it reaches the inside of the membrane. This is encouraging, but it must be mentioned that a physical theory of this kind does not lead to satisfactory functions for α_h and β_h without further *ad hoc* assumptions.

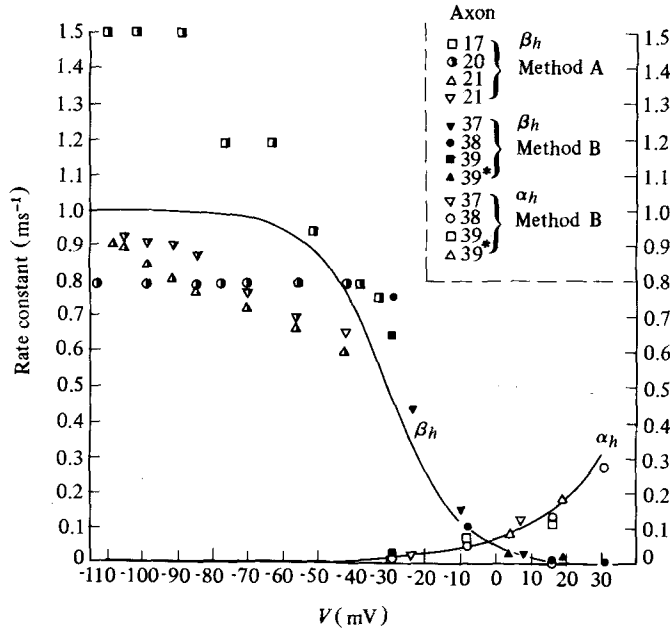


Figure 9. Rate constants of inactivation (α_h and β_h) as functions of membrane potential (V). The smooth curves were calculated from equations (23) and (24). The experimental values of α_h and β_h were obtained from data such as those in Table 2 of this paper (method A) or from the values of τ_h and h_∞ given in Table 1 of Hodgkin and Huxley (1952c) (method B). Temperature differences were allowed for by scaling with a Q_{10} of 3. Axon 39 was at 19°C; all others at 3–9°C. The values for axons 37 and 39* were displaced by -1.5 and -12 mV in order to give $h_\infty = 0.6$ at $V = 0$.

3. Reconstruction of Nerve Behaviour. The remainder of this paper will be devoted to calculations of the electrical behaviour of a model nerve whose properties are defined by the equations which were fitted in Section 2 to the voltage clamp records described in the earlier papers of this series.

3.1. Summary of equations and parameters. We may first collect the equations which give the total membrane current I as a function of time and voltage. These are:

$$I = C_M \frac{dV}{dt} + \bar{g}_K n^4 (V - V_K) + \bar{g}_{Na} m^3 h (V - V_{Na}) + \bar{g}_1 (V - V_1), \quad (26)$$

where:

$$dn/dt = \alpha_n(1-n) - \beta_n n, \quad (7)$$

$$dm/dt = \alpha_m(1-m) - \beta_m m, \quad (15)$$

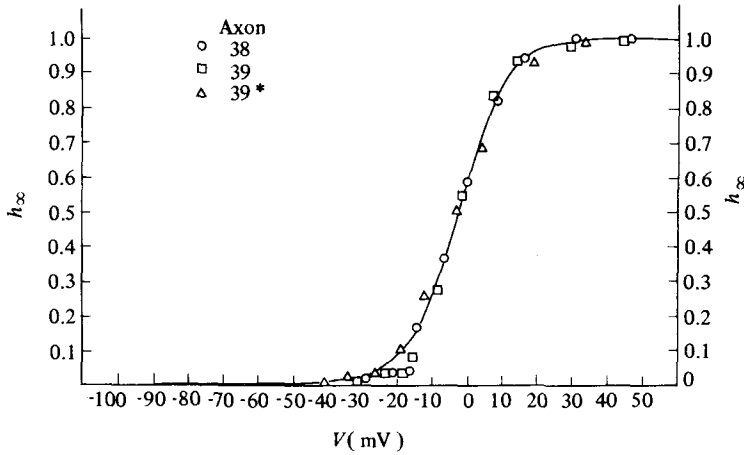


Figure 10. Steady state relation between h and V . The smooth curve is drawn according to equation (25). The experimental points are those given in Table 1 of Hodgkin and Huxley (1952c). Axon 38 (5°C) as measured. Axon 39 (19°C) displaced -1.5 mV. Axon 39* (3°C , fibre in derelict state) displaced -12 mV. The curve gives the fraction of the sodium-carrying system which is readily available, as a function of membrane potential, in the steady state.

$$dh/dt = \alpha_h(1-h) - \beta_h h, \quad (16)$$

and:

$$\alpha_n = 0.01(V+10) / \left(\exp \frac{V+10}{10} - 1 \right), \quad (12)$$

$$\beta_n = 0.125 \exp(V/80), \quad (13)$$

$$\alpha_m = 0.1(V+25) / \left(\exp \frac{V+25}{10} - 1 \right), \quad (20)$$

$$\beta_m = 4 \exp(V/18), \quad (21)$$

$$\alpha_h = 0.07 \exp(V/20), \quad (23)$$

$$\beta_h = 1 / \left(\exp \frac{V+30}{10} + 1 \right). \quad (24)$$

Equation (26) is derived simply from equations (1)–(6) and (14) in Section 2. The four terms on the right-hand side give respectively the capacity current, the current carried by K^+ ions, the current carried by Na^+ ions and the leak current, for 1 cm^2 of membrane. These four components are in parallel and add up to give the total current density through the membrane I . The conductances

to K and Na are given by the constants \bar{g}_K and \bar{g}_{Na} , together with the dimensionless quantities n , m and h , whose variation with time after a change of membrane potential is determined by the three subsidiary equations (7), (15) and (16). The α 's and β 's in these equations depend only on the instantaneous value of the membrane potential, and are given by the remaining six equations.

Potentials are given in mV, current density in $\mu\text{A cm}^{-2}$, conductances in m mho cm^{-2} , capacity in $\mu\text{F cm}^{-2}$, and time in ms. The expressions for the α 's and β 's are appropriate to a temperature of 6.3°C ; for other temperatures they must be scaled with a Q_{10} of 3.

The constants in equation (26) are taken as independent of temperature. The values chosen are given in Table 3, column 2, and may be compared with the experimental values in columns 3 and 4.

3.2. Membrane currents during a voltage clamp. Before applying equation (26) to the action potential it is well to check that it predicts correctly the total current during a voltage clamp. At constant voltage $dV/dt=0$ and the coefficients α and β are constant. The solution is then obtained directly in terms of the expressions already given for n , m and h [equations (8), (17) and (18)]. The total ionic current was computed from these for a number of different voltages and is compared with a series of experimental curves in Fig. 11. The only important difference is that the theoretical current has too little delay at the sodium potential; this reflects the inability of our equations to account fully for the delay in the rise of g_K (pp. 34–35; p. 509 of original paper).

3.3. "Membrane" and propagated action potentials. By a "membrane" action potential is meant one in which the membrane potential is uniform, at each instant, over the whole of the length of fibre considered. There is no current along the axis cylinder and the net membrane current must therefore always be zero, except during the stimulus. If the stimulus is a short shock at $t=0$, the form of the action potential should be given by solving equation (26) with $I=0$ and the initial conditions that $V=V_0$ and m , n and h have their resting steady-state values, when $t=0$.

The situation is more complicated in a propagated action potential. The fact that the local circuit currents have to be provided by the net membrane current leads to the well-known relation:

$$i = \frac{1}{r_1 + r_2} \frac{\partial^2 V}{\partial x^2}, \quad (27)$$

where i is the membrane current per unit length, r_1 and r_2 are the external and internal resistances per unit length, and x is distance along the fibre. For an axon surrounded by a large volume of conducting fluid, r_1 is negligible compared with r_2 . Hence:

Table 3.

Constant	Value chosen	Experimental values			Reference
		Mean	Range		
C_M ($\mu\text{F cm}^{-2}$)	1.0	0.91	0.8 to 1.5	Table 1, Hodgkin <i>et al.</i> (1952)	
V_{Na} (mV)	-115	-109	-95 to -119	p. 455, Hodgkin and Huxley (1952a)	
V_K (mV)	-12	-11	+9 to +14	Table 3, values for low temperature in sea water, Hodgkin and Huxley (1952b)	
V_l (mV)	-10 to 613*	-11	-4 to -22	Table 5, Hodgkin and Huxley (1952b)	
\bar{g}_{Na} (m mho cm^{-2})	120	{ 80 160	65 to 90 120 to 260	Fully analysed results, Table 2† } Hodgkin and Huxley (1952a)	
\bar{g}_K (m mho cm^{-2})	36	34	26 to 49	p. 463, Hodgkin and Huxley (1952a)	
\bar{g}_l (m mho cm^{-2})	0.3	0.26	0.13 to 0.50	Table 5, Hodgkin and Huxley (1952b)	

* Exact value chosen to make the total ionic current zero at the resting potential ($V = 0$).

† The experimental values for \bar{g}_{Na} were obtained by multiplying the peak sodium conductances by factors derived from the values chosen for α_m , β_m , α_h , and β_h .

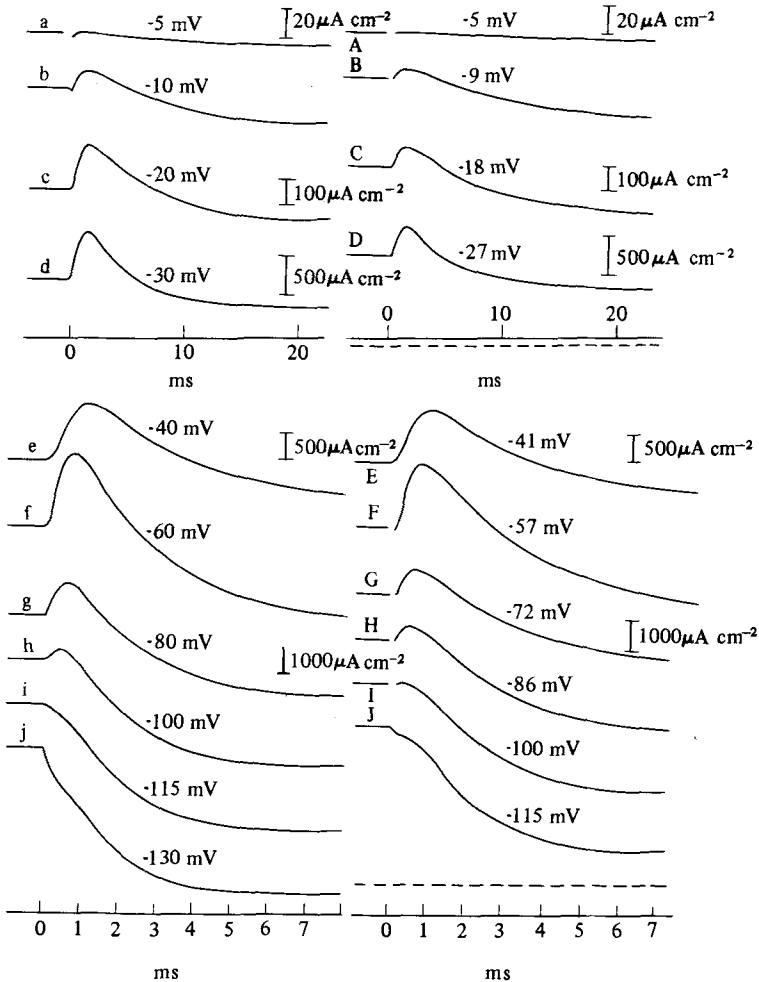


Figure 11. Left-hand column: time course of membrane current during voltage clamp, calculated for temperature of 4°C from equation (26) and subsidiaries and plotted on the same scale as the experimental curves in the right-hand column. Right-hand column: observed time course of membrane currents during voltage clamp. Axon 31 at 4°C ; compensated feedback. The time scale changes between d, D and e, E. The current scale changes after b, B; c, C; d, D and f, F.

$$i = \frac{1}{r_2} \frac{\partial^2 V}{\partial x^2},$$

or:

$$I = \frac{a}{2R_2} \frac{\partial^2 V}{\partial x^2}, \quad (28)$$

where I is the membrane current density, a is the radius of the fibre and R_2 is the

specific resistance of the axoplasm. Inserting this relation in equation (26), we have:

$$\frac{a}{2R_2} \frac{\partial^2 V}{\partial x^2} = C_M \frac{\partial V}{\partial t} + \bar{g}_K n^4 (V - V_K) + \bar{g}_{Na} m^3 h (V - V_{Na}) + \bar{g}_1 (V - V_1), \quad (29)$$

the subsidiary equations being unchanged.

Equation (29) is a partial differential equation, and it is not practicable to solve it as it stands. During steady propagation, however, the curve of V against time at any one position is similar in shape to that of V against distance at any one time, and it follows that:

$$\frac{\partial^2 V}{\partial x^2} = \frac{1}{\theta^2} \frac{\partial^2 V}{\partial t^2},$$

where θ is the velocity of conduction. Hence:

$$\frac{a}{2R_2 \theta^2} \frac{d^2 V}{dt^2} = C_M \frac{dV}{dt} + \bar{g}_K n^4 (V - V_K) + \bar{g}_{Na} m^3 h (V - V_{Na}) + \bar{g}_1 (V - V_1). \quad (30)$$

This is an ordinary differential equation and can be solved numerically, but the procedure is still complicated by the fact that θ is not known in advance. It is necessary to guess a value of θ , insert it in equation (30) and carry out the numerical solution starting from the resting state at the foot of the action potential. It is then found that V goes off towards either $+\infty$ or $-\infty$, according to whether or not the guessed θ was too small or too large. A new value of θ is then chosen and the procedure repeated, and so on. The correct value brings V back to zero (the resting condition) when the action potential is over.

The solutions which go towards $\pm\infty$ correspond to action potentials travelling slower than normal under a travelling anode or faster than normal under a travelling cathode. We suspect that a system which tends to $-\infty$ for all values of θ after an initial negative displacement of V is one which is incapable of propagating an action potential.

4. Numerical Methods

4.1. Membrane action potentials

4.1.1. Integration procedure. The equations to be solved are the four simultaneous first-order equations (26), (7), (15), and (16) (pp. 43–44; p. 518 of original paper). After slight rearrangement (which will be omitted in this description) these were integrated by the method of Hartree (1932/3). Denoting the beginning and end of a step by t_0 and $t_1 (= t_0 + \delta t)$ the procedure for each step was as follows.

- (1) Estimate V_1 from V_0 and its backward differences.

- (2) Estimate n_1 from n_0 and its backward differences.
- (3) Calculate $(dn/dt)_1$ from equation (7) using the estimated n_1 and the values of α_n and β_n appropriate to the estimated V_1 .
- (4) Calculate n_1 from the equation:

$$n_1 - n_0 = \frac{\delta t}{2} \left\{ \left(\frac{dn}{dt} \right)_0 + \left(\frac{dn}{dt} \right)_1 - \frac{1}{12} \left[\Delta^2 \left(\frac{dn}{dt} \right)_0 + \Delta^2 \left(\frac{dn}{dt} \right)_1 \right] \right\},$$

$\Delta^2(dn/dt)$ is the second difference of dn/dt ; its value at t_1 has to be estimated.

- (5) If this value of n_1 differs from that estimated in (2), repeat (3) and (4) using the new n_1 . If necessary, repeat again until successive values of n_1 are the same.
- (6) Find m_1 and h_1 by procedures analogous to steps (2)–(5).
- (7) Calculate $\bar{g}_K n_1^4$ and $\bar{g}_{Na} m_1^3 h_1$.
- (8) Calculate $(dV/dt)_1$ From equation (26) using the values found in (7) and the originally estimated V_1 .
- (9) Calculate a corrected V_1 by procedures analogous to steps (4) and (5). This result never differed enough from the original estimated value to necessitate repeating the whole procedure from step (3) onwards.

The step value had to be very small initially (since there are no differences at $t=0$) and it also had to be changed repeatedly during a run, because the differences became unmanageable if it was too large. It varied between about 0.01 ms at the beginning of a run or 0.02 ms during the rising phase of the action potential, and 1 ms during the small oscillations which follow the spike.

4.1.2. Accuracy. The last digit retained in V corresponded to microvolts. Sufficient digits were kept in the other variables for the resulting errors in the change of V at each step to be only occasionally as large as 1 μ V. It is difficult to estimate the degree to which the errors at successive steps accumulate, but we are confident that the overall errors are not large enough to be detected in the illustrations of this paper.

4.1.3. Temperature differences. In calculating the action potential it was convenient to use tables giving the α 's and β 's at intervals of 1 mV. The tabulated values were appropriate to a fibre at 6.3°C. To obtain the action potential at some other temperature T '°C the direct method would be to multiply all α 's and β 's by a factor $\phi = 3^{(T-6.3)/10}$, this being correct for a Q_{10} of 3. Inspection of equation (26) shows that the same result is achieved by calculating the action potential at 6.3°C with a membrane capacity of $\phi C_M \mu\text{F cm}^{-2}$, the unit of time being $1/\phi$ ms. This method was adopted since it saved recalculating the tables.

4.2. Propagated action potential

4.2.1. Equations. The main equation for a propagated action potential is equation (30). Introducing a quantity $K=2R_2\theta^2C_M/a$, this becomes:

$$\frac{d^2V}{dt^2} = K \left\{ \frac{dV}{dt} + \frac{1}{C_M} [\bar{g}_K n^4 (V - V_K) + \bar{g}_{Na} m^3 h (V - V_{Na}) + \bar{g}_1 (V - V_1)] \right\}. \quad (31)$$

The subsidiary equations (7), (15) and (16), and the α 's and β 's, are the same as for the membrane equation.

4.2.2. Integration procedure. Steps (1)–(7) were the same as for the membrane action potential. After that the procedure was as follows.

- (8) Estimate $(dV/dt)_1$ from $(dV/dt)_0$ and its backward differences.
- (9) Calculate $(d^2V/dt^2)_1$ from equation (31), using the values found in (7) and the estimated values of V_1 and $(dV/dt)_1$.
- (10) Calculate a corrected $(dV/dt)_1$ by procedures analogous to steps (4) and (5).
- (11) Calculate a corrected V_1 by a procedure analogous to step (4), using the corrected $(dV/dt)_1$.
- (12) If necessary, repeat (9)–(11) using the new V_1 and $(dV/dt)_1$, until successive values of V_1 agree.

4.2.3. Starting conditions. In practice it is necessary to start with V deviating from zero by a finite amount (0.1 mV) was used). The first few values of V , and hence the differences, were obtained as follows. Neglecting the changes in g_K and g_{Na} , equation (31) is:

$$\frac{d^2V}{dt^2} = K \left\{ \frac{dV}{dt} + \frac{g_0}{C_M} V \right\},$$

where g_0 is the resting conductance of the membrane. The solution of this equation is $V = V_0 e^{\mu t}$, where μ is a solution of:

$$\mu^2 - K\mu - Kg_0/C_M = 0. \quad (32)$$

When K has been chosen, μ can thus be found and hence V_1, V_2 , etc. ($V_0 e^{\mu t_1}$, $V_0 e^{\mu t_2}$, etc.).

After several runs had been calculated, so that K was known within fairly narrow limits, time was saved by starting new runs not from near $V=0$ but from a set of values interpolated between corresponding points on a run which had gone towards $+\infty$ and another which had gone towards $-\infty$.

4.2.4. Choice of K . The value of K chosen for the first run makes no difference to the final result, but the nearer it is to the correct value the fewer

runs will need to be evaluated. The starting value was found by inserting in equation (32) a value of u found by measuring the foot of an observed action potential.

4.2.5. Calculation of falling phase. The procedure outlined above is satisfactory for the rising phase and peak of the action potential but becomes excessively tedious in the falling phase and the oscillations which follow the spike. A different method, which for other reasons is not applicable in the earlier phases, was therefore employed. The solution was continued as a membrane action potential, and the value of d^2V/dt^2 calculated at each step from the differences of dV/dt . From these it was possible to derive an estimate of the values (denoted by z) that d^2V/dt^2 would have taken in a propagated action potential. The membrane solution was then re-calculated using the following equation instead of equation (31):

$$\frac{dV}{dt} = -\frac{1}{C_M} \{ \bar{g}_K n^4 (V - V_K) + \bar{g}_{Na} m^3 h (V - V_{Na}) + \bar{g}_I (V - V_I) \} + \frac{z}{K}. \quad (33)$$

This was repeated until the z 's assumed for a particular run agreed with the d^2V/dt^2 's derived from the same run. When this is the case, equation (33) is identical to equation (31), the main equation for the propagated action potential.

5. Results

5.1. Membrane action potentials

5.1.1. Form of action potential at 6°C. Three calculated membrane action potentials, with different strengths of stimulus, are shown in the upper part of Fig. 12. Only one, in which the initial displacement of membrane potential was 15 mV, is complete; in the other two the calculation was not carried beyond the middle of the falling phase because of the labour involved and because the solution had become almost identical with the 15 mV action potential, apart from the displacement in time. One solution for a stimulus just below threshold is also shown.

The lower half of Fig. 12 shows a corresponding series of experimental membrane action potentials. It will be seen that the general agreement is good, as regards amplitude, form and time-scale. The calculated action potentials do, however, differ from the experimental in the following respects: (1) the drop during the first 0.1 ms is smaller; (2) the peaks are sharper; (3) there is a small hump in the lower part of the falling phase; (4) the ending of the falling phase is too sharp. The extent to which these differences are the result of known shortcomings in our formulation will be discussed on pp. 69–70; pp. 542–543 of original paper).

The positive phase of the calculated action potential has approximately the

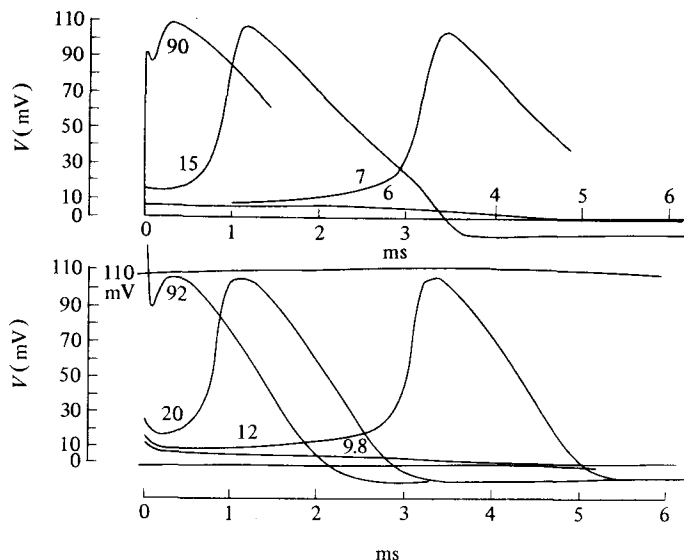


Figure 12. Upper family: solutions of equation (26) for initial depolarizations of 90, 15, 7 and 6 mV (calculated for 6°C). Lower family: tracings of membrane action potentials recorded at 6°C from axon 17. The numbers attached to the curves give the shock strength in $\text{m} \mu\text{C cm}^{-2}$. The vertical and horizontal scales are the same in both families (apart from the slight curvature indicated by the 110 mV calibration line). In this and all subsequent figures depolarizations (or negative displacements of V) are plotted upwards.

correct form and duration, as may be seen from Fig. 13 in which a pair of curves are plotted on a slower time scale.

Certain measurements of these and other calculated action potentials are collected in Table 4.

5.1.2. Form of action potential at 18.5°C. Figure 14 shows a comparison between a calculated membrane action potential at 18.5°C and an experimental one at 20.5°C. The same differences can be seen as at the low temperature, but, except for the initial drop, they are less marked. In both the calculated and the experimental case, the rise of temperature has greatly reduced the duration of the spike, the difference being more marked in the falling than in the rising phase (Table 4), as was shown in propagated action potentials by Hodgkin and Katz (1949).

The durations of both falling phase and positive phase are reduced at the higher temperature by factors which are not far short of that (3.84) by which the rate constants of the permeability changes are raised ($Q_{10} = 3.0$). This is the justification for the differences in time scale between the upper and lower parts in Figs 13 and 14.

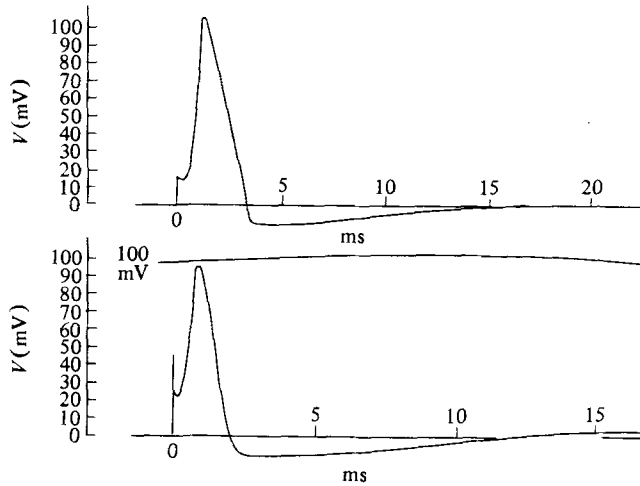


Figure 13. Upper curve: solution of equation (26) for initial depolarization of 15 mV, calculated for 6°C. Lower curve: tracing of membrane action potential recorded at 9.1°C (axon 14). The vertical scales are the same in both curves (apart from curvature in the lower record). The horizontal scales differ by a factor appropriate to the temperature difference.

5.2. Propagated action potential

5.2.1. Form of propagated action potential. Figure 15 compares the calculated propagated action potential, at 18.5°C, with experimental records on both fast and slow time bases. As in the case of the membrane action potential, the only differences are in certain details of the form of the spike.

5.2.2. Velocity of conduction. The value of the constant K that was found to be needed in the equation for the propagated action potential [equation (31)] was 10.47 ms^{-1} . This constant, which depends only on properties of the membrane, determines the conduction velocity in conjunction with the constants of the nerve fibre considered as a cable. The relation is given by the definition of K (p. 50; p. 524 of original paper), from which:

$$\theta = \sqrt{(Ka/2R_2C_M)}, \quad (34)$$

where θ = conduction velocity, a = radius of axis cylinder, R_2 = specific resistance of axoplasm, and C_M = capacity per unit area of membrane.

The propagated action potential was calculated for the temperature at which the record C of Fig. 15 was obtained, and with the value of C_M ($1.0 \mu\text{F cm}^{-2}$) that was measured on the fibre from which that record was made. Since θ , a and R_2 were also measured on that fibre, a direct comparison between calculated and observed velocities is possible. The values of a and R_2 were 238μ and $35.4 \Omega \text{ cm}$ respectively. Hence the calculated conduction velocity is:

Table 4. Characteristics of calculated action potentials

Type of action potential	Temperature (°C)	Stimulus	Spike height (mV)	Amplitude of positive phase (mV)	Peak conductance (m mho cm ⁻²)	Duration of rising phase, 20 mV to peak (ms)	Duration of falling phase, peak to V=0 (ms)	Duration of positive phase (ms)	Interval from peak of potential to peak of conductance (ms)	Max. rate of rise (V s ⁻¹)
Propagated Membrane	18.5	—	90.5	9.7	32.6	0.252	0.67	5.20	-0.016	431
Membrane	18.5	15 mV depolarization	96.8	10.5	30.7	0.275	0.61	5.09	+0.012	364
Membrane	6.3	100 mV depolarization	108.8	—	45.5	—	—	—	+0.16	—
Membrane	6.3	90 mV depolarization	108.5	—	44.8	—	—	—	+0.15	—
Membrane	6.3	15 mV depolarization	105.4	11.2	37.0	0.59	2.21	14.15	+0.15	311
Membrane	6.3	7 mV depolarization	102.1	—	33.4	0.62	—	—	+0.16	277
Membrane	6.3	Anode break	112.1	11.2	53.4	0.50	2.54	14.4	+0.14	414

$$(10470 \times 0.0238/2 \times 35.4 \times 10^{-6})^{1/2} \text{ cm s}^{-1} = 18.8 \text{ ms}^{-1}.$$

The velocity found experimentally in this fibre was 21.2 ms^{-1} .

5.3. Impedance changes

5.3.1. Time course of conductance change. Cole and Curtis (1939) showed that the impedance of the membrane fell during a spike, and that the fall was

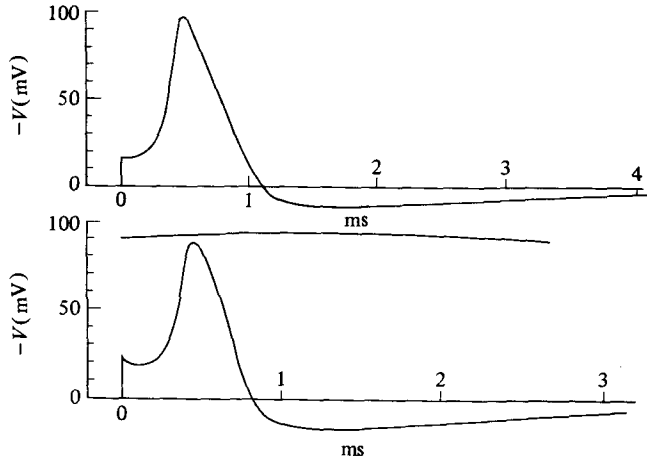


Figure 14. Upper curve: solution of equation (26) for initial depolarization of 15 mV, calculated for 18.5°C . Lower curve: tracing of membrane action potential recorded at 20.5°C (axon 11). Vertical scales are similar. Horizontal scales differ by a factor appropriate to the temperature difference.

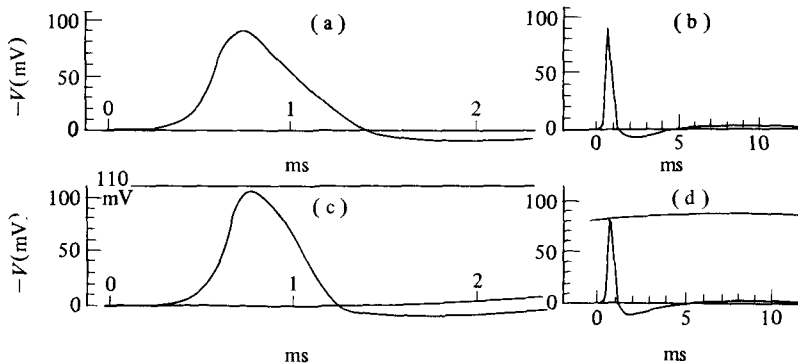


Figure 15. (a) Solution of equation (31) calculated for K of 10.47 ms^{-1} and temperature of 18.5°C . (b) Same solution plotted on slower time scale. (c) Tracing of propagated action potential on same vertical and horizontal scales as (a). Temperature 18.5°C . (d) Tracing of propagated action potential from another axon on approximately the same vertical and horizontal scales as (b). Temperature 19.2°C . This axon had been used for several hours; its spike was initially 100 mV.

due to a great increase in the conductance which is in parallel with the membrane capacity. An effect of this kind is to be expected on our formulation, since the entry of Na^+ which causes the rising phase, and the loss of K^+ which causes the falling phase, are consequent on increases in the conductance of the membrane to currents carried by these ions. These component conductances are evaluated during the calculation, and the total conductance is obtained by adding them and the constant "leak conductance", \bar{g}_l .

Figure 16a shows the membrane potential and conductance in a calculated membrane action potential. For comparison, Fig. 16b shows superposed records of potential and impedance bridge output (proportional to conductance change), taken from Cole and Curtis's paper. The time scale is the same in b as in a, and the curves have been drawn with the same peak height. It will be seen that the main features of Cole and Curtis's record are reproduced in the calculated curve. Thus: (1) the main rise in conductance begins later than the rise of potential; (2) the conductance does not fall to its resting value until late in the positive phase; (3) the peak of the conductance change occurs at nearly the same time as the peak of potential. The exact time relation between the peaks depends on the conditions, as can be seen from Table 4.

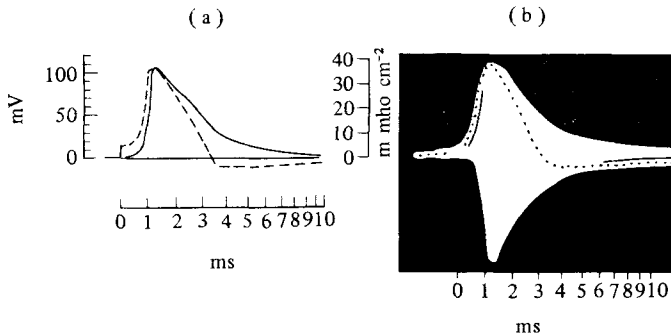


Figure 16. (a) Solution of equation (26) for initial depolarization of 15 mV at a temperature of 6°C . The broken curve shows the membrane action potential in mV; the continuous curve shows the total membrane conductance ($g_{\text{Na}} + g_{\text{K}} + \bar{g}_l$) as a function of time. (b) Records of propagated action potential (dotted curve) and conductance change reproduced from Cole and Curtis (1939). The time scales are the same in (a) and (b).

We chose a membrane action potential for the comparison in Fig. 16 because the spike duration shows that the experimental records were obtained at about 6°C , and our propagated action potential was calculated for 18.5°C . The conductance during the latter is plotted together with the potential in Fig. 17. The same features are seen as in the membrane action potential, the

delay between the rise of potential and the rise of conductance being even more marked.

5.3.2. Absolute value of peak conductance. The agreement between the height of the conductance peak in Fig. 16a and the half-amplitude of the bridge output in Fig. 16b is due simply to the choice of scale. Nevertheless, our calculated action potentials agree well with Cole and Curtis's results in this respect. These authors found that the average membrane resistance at the peak of the impedance change was $25 \Omega \text{ cm}^2$, corresponding to a conductance of 40 m mho cm^{-2} . The peak conductances in our calculated action potentials ranged from 31 to 53 m mho cm^{-2} according to the conditions, as shown in Table 4.

5.3.3. Components of conductance change. The manner in which the conductances to Na^+ and K^+ contribute to the change in total conductance is shown in Fig. 17 for the calculated propagated action potential. The rapid rise

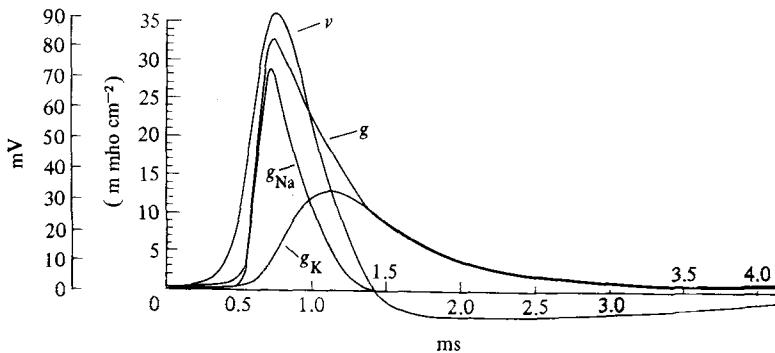


Figure 17. Numerical solution of equation (31) showing components of membrane conductance (g) during propagated action potential ($-V$). Details of the analysis are as in Fig. 15.

is due almost entirely to sodium conductance, but after the peak the potassium conductance takes a progressively larger share until, by the beginning of the positive phase, the sodium conductance has become negligible. The tail of raised conductance that falls away gradually during the positive phase is due solely to potassium conductance, the small constant leak conductance being of course present throughout.

5.4. Ionic movements

5.4.1. Time course of ionic currents. The time course of the components of membrane current carried by sodium and potassium ions during the calculated propagated spike is shown in Fig. 18c. The total ionic current contains also a

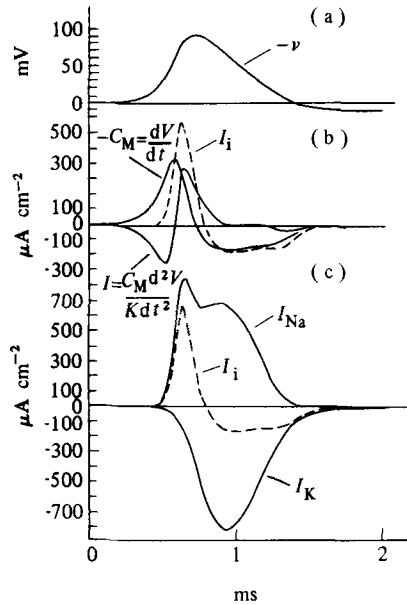


Figure 18. Numerical solution of equation (31) showing components of membrane current during propagated action potential: (a) membrane potential ($-V$); (b) ionic current (I_i), capacity current ($-C_M(dV/dt)$) and total membrane current ($I = (C_M/K)(d^2V/dt^2)$); (c) ionic current (I_i), sodium current (I_{Na}) and potassium current (I_K). The time scale applies to all the curves. Details of the analysis are as in Fig. 15.

small contribution from "leak current" which is carried into the axis cylinder by ions crossing the membrane: it may leave the axis cylinder again by altering the charge on the membrane capacity, or it may turn either way along the axis cylinder making a net contribution, I , to the local circuit current. The magnitudes of these two terms during steady propagation are $-C_M dV/dt$ and $(C_M/K) d^2V/dt^2$ respectively, and the manner in which the ionic current is divided between them at the different stages of the spike is shown in Fig. 18b. It will be seen that the ionic current is very small until the potential is well beyond the threshold level, which is shown by Fig. 12a to be about 6 mV. During this period the current for charging the membrane capacity comes almost entirely from local circuits. The fact that the ionic current does not become appreciable as soon as the threshold depolarization is passed is due partly to the smallness of the currents reached in any circumstances near the threshold, and partly to the delay with which sodium conductance rises when the potential is lowered.

5.4.2. Total movements of ions. The total entry of sodium and loss of potassium can be obtained by integrating the corresponding ionic currents over the whole impulse. This has been done for the four complete action

potentials that we calculated, and the results are given in Table 5. It will be seen that the results at 18.5°C are in good agreement with the values found experimentally by Keynes (1951) and Keynes and Lewis (1951), which were obtained at comparable temperatures.

5.4.3. Ionic fluxes. The flux in either direction of an ion can be obtained from the net current and the equilibrium potential for that ion, if the independence principle (Hodgkin and Huxley, 1952a) is assumed to hold. Thus the outward flux of sodium ions is $I_{\text{Na}}/(\exp(V - V_{\text{Na}})F/RT - 1)$, and the inward flux of potassium ions is $-I_{\text{K}}/(\exp(V_{\text{K}} - V)F/RT - 1)$. These two quantities were evaluated at each step of the calculated action potentials, and integrated over the whole impulse. The integrated flux in the opposite direction is given in each case by adding the total net movement. The results are given in Table 5, where they can be compared with the results obtained with radioactive tracers by Keynes (1951) on *Sepia* axons. It will be seen that our theory predicts too little exchange of Na and too much exchange of K during an impulse. This discrepancy will be discussed later.

5.5. Refractory period

5.5.1. Time course of inactivation and delayed rectification. According to our theory, there are two changes resulting from the depolarization during a spike which make the membrane unable to respond to another stimulus until a certain time has elapsed. These are "inactivation", which reduces the level to which the sodium conductance can be raised by a depolarization, and the delayed rise in potassium conductance, which tends to hold the membrane potential near to the equilibrium value for potassium ions. These two effects are shown in Fig. 19 for the calculated membrane action potential at 6°C. Both curves reach their normal levels again near the end of the positive phase, and finally settle down after a heavily damped oscillation of small amplitude which is not seen in the figure.

5.5.2. Responses to stimuli during positive phase. We calculated the responses of the membrane when it was suddenly depolarized by 90 mV at various times during the positive phase of the membrane action potential at 6°C. These are shown by the upper curves in Fig. 20. After the earliest stimulus the membrane potential falls again with hardly a sign of activity, and the membrane can be said to be in the "absolute refractory period". The later stimuli produce action potentials of increasing amplitude, but still smaller than the control; these are in the "relative refractory period". Corresponding experimental curves are shown in the lower part of Fig. 20. The agreement is good, as regards both the duration of the absolute refractory period and the changes in shape of the spike as recovery progresses.

Table 5. Ionic movements during an impulse

Type of action potential	Temp. (°C)	Stimulus (mV)	Sodium			Potassium		
			Influx	Outflux	Net entry	Influx	Outflux	Net loss
Theoretical (<i>Loligo</i>):								
(1) Propagated Membrane	18.5	—	5.42	1.09	4.33	1.72	5.98	4.26
(2) Membrane	18.5	15	5.01	1.02	3.99	1.71	5.78	4.07
(3) Membrane	6.3	15	19.30	4.84	14.46	6.17	20.49	14.32
(4) Membrane	6.3	Anode break	26.61	9.45	17.16	6.64	23.41	16.77
Experimental:								
(5) Propagated (<i>Loligo</i>)	—	—	—	—	3.5	—	—	3.0
(6) Propagated (<i>Sepia</i>)	14	—	10.3	6.6	3.7	0.39	4.7	4.3
(7) Propagated (<i>Sepia</i>)	—	—	—	—	3.8	—	—	3.6

All values are expressed in $\mu\text{mol cm}^{-2}$ and represent the excess over the corresponding movement in the resting state. In the theoretical cases the integration is taken as far as the third intersection with the base line after the spike; it is begun in case (1) when $V=0.1$ mV; (2) and (3) at the stimulus; (4) when $V=0$ before the spike. Experimental data from Keynes (1951) for row 6 and from Keynes and Lewis (1951) for rows 5 and 7.

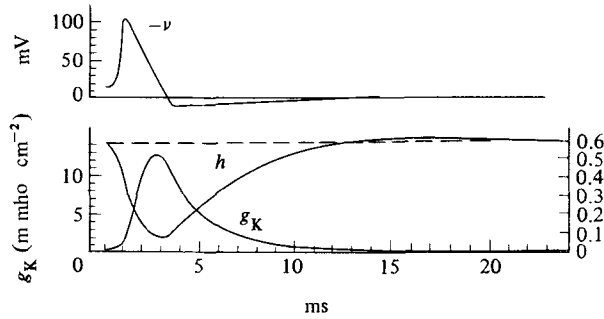


Figure 19. Numerical solution of equation (26) for initial depolarization of 15 mV and temperature of 6°C. Upper curve: membrane potential, as in Fig. 13. Lower curves show time course of g_K and h during action potential and refractory period.

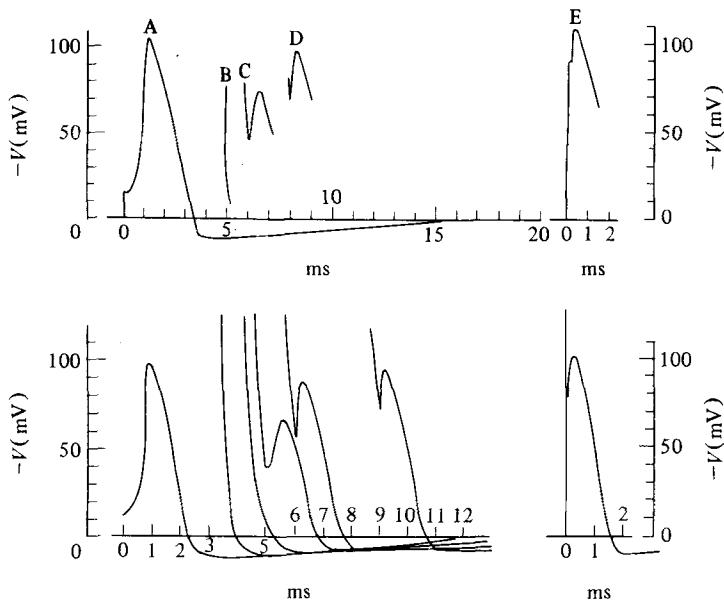


Figure 20. Theoretical basis of refractory period. Upper curves: numerical solutions of equation (26) for temperature of 6°C. Curve A gives the response to $15 \text{ m } \mu\text{C cm}^{-2}$ applied instantaneously at $t=0$. Curve E gives the response to $90 \text{ m } \mu\text{C cm}^{-2}$ again applied in the resting state. Curves B–D show effect of applying $90 \text{ m } \mu\text{C cm}^{-2}$ at various times after curve A. Lower curves: a similar experiment with an actual nerve, temperature 9°C. The voltage scales are the same throughout. The time scales differ by a factor appropriate to the temperature difference.

5.6. *Excitation.* Our calculations of excitation processes were all made for the case where the membrane potential is uniform over the whole area considered, and not for the case of local stimulation of a whole nerve. There were two reasons for this: first, that such data from the squid giant fibre as we had for comparison were obtained by uniform stimulation of the membrane with the long electrode; and, secondly, that calculations for the whole nerve case would have been extremely laborious since the main equation is then a partial differential equation.

5.6.1. *Threshold.* The curves in Figs 12 and 21 show that the theoretical "membrane" has a definite threshold when stimulated by a sudden displacement of membrane potential. Since the initial fall after the stimulus is much less marked in these than in the experimental curves, it is relevant to compare the lowest point reached in a just threshold curve, rather than the magnitude of the original displacement. In the calculated series this is about 6 mV and in the experimental about 8 mV. This agreement is satisfactory, especially as the value for the calculated series must depend critically on such things as the leak conductance, whose value was not very well determined experimentally.

The agreement might have been somewhat less good if the comparison had been made at a higher temperature. The calculated value would have been much the same, but the experimental value in the series at 23°C shown in Fig. 8 of Hodgkin *et al.* (1952) is about 15 mV. However, this fibre had been stored for 5 hr before use and was therefore not in exactly the same state as those on which our measurements were based.

5.6.2. *Subthreshold responses.* When the displacement of membrane potential was less than the threshold for setting up a spike, characteristic subthreshold responses were seen. One such response is shown in Fig. 12, while several are plotted on a larger scale in Fig. 21b. Figure 21a shows for comparison the corresponding calculated responses of our model. The only appreciable differences, in the size of the initial fall and in the threshold level, have been mentioned already in other connections.

During the positive phase which follows each calculated subthreshold response, the potassium conductance is raised and there is a higher degree of "inactivation" than in the resting state. The threshold must therefore be raised in the same way as it is during the relative refractory period following a spike. This agrees with the experimental findings of Pumphrey *et al.* (1940).

5.6.3. *Anode break excitation.* Our axons with the long electrode in place often gave anode break responses at the end of a period during which current was made to flow inward through the membrane. The corresponding response of our theoretical model was calculated for the case in which a current sufficient

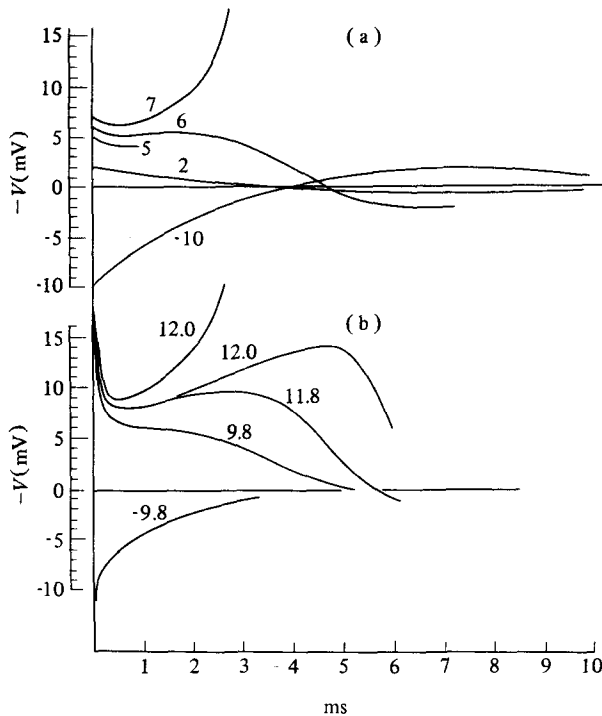


Figure 21. (a) Numerical solutions of equation (26) for 6°C. The numbers attached to the curves give the initial depolarization in mV (also the quantity of charge applied in $\text{m } \mu\text{C cm}^{-2}$). (b) Response of nerve membrane at 6°C to short shocks; the numbers show the charge applied in $\text{m } \mu\text{C cm}^{-2}$. The curves have been replotted from records taken at low amplification and a relatively high time-base speed.

to bring the membrane potential to 30 mV above the resting potential was suddenly stopped after passing for a time long compared with all the time-constants of the membrane. To do this, equation (26) was solved with $I=0$ and the initial conditions that $V = +30$ mV, and m , n and h have their steady-state values for $V = +30$ mV, when $t=0$. The calculation was made for a temperature of 6.3°C. A spike resulted, and the time course of membrane potential is plotted in Fig. 22a. A tracing of an experimental anode break response is shown in Fig. 22b; the temperature is 18.5°C, no record near 6° being available. It will be seen that there is good general agreement. (The oscillations after the positive phase in Fig. 22b are exceptionally large; the response of this axon to a small constant current was also unusually oscillatory as shown in Fig. 23.)

The basis of the anode break excitation is that anodal polarization decreases the potassium conductance and removes inactivation. These effects persist for an appreciable time so that the membrane potential reaches its resting value with a reduced outward potassium current and an increased inward sodium

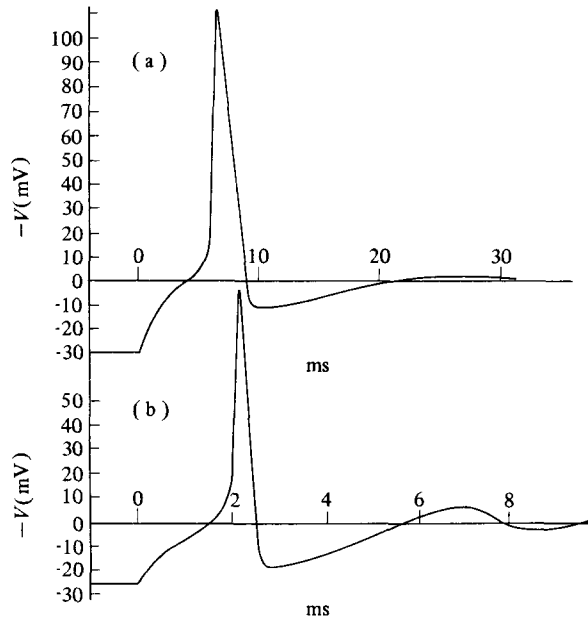


Figure 22. Theoretical basis of anode break excitation: (a) numerical solution of equation (26) for boundary condition $-V = -30$ mV for $t < 0$ (temperature 6°C); (b) anode break excitation following sudden cessation of external current which had raised the membrane potential by 26.5 mV (giant axon with long electrode at 18.5°C). Time scales differ by a factor appropriate to the temperature difference.

current. The total ionic current is therefore inward at $V=0$ and the membrane undergoes a depolarization which rapidly becomes regenerative.

5.6.4. Accommodation. No measurements of accommodation were made nor did we make any corresponding calculations for our model. It is clear, however, that the model will show "accommodation" in appropriate cases. This may be shown in two ways. Firstly, during the passage of a constant cathodal current through the membrane, the potassium conductance and the degree of inactivation will rise, both factors raising the threshold. Secondly, the steady-state ionic current at all strengths of depolarization is outward (Fig. 11), so that an applied cathodal current which rises sufficiently slowly will never evoke a regenerative response from the membrane, and excitation will not occur.

5.7. Oscillations. In all the calculated action potentials and subthreshold responses the membrane potential finally returns to its resting value with a heavily damped oscillation. This is well seen after subthreshold stimuli in

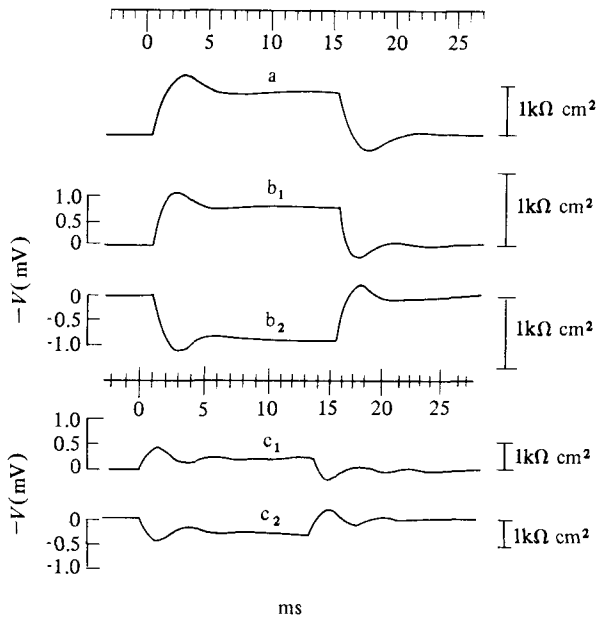


Figure 23. (a) Solution of equation (35) for small constant current pulse; temperature 18.5°C ; linear approximation. The curve shows $\delta V/\delta I$ (plotted upwards) as a function of time. (b) Changes in membrane potential associated with application of weak constant currents of duration 15 ms and strength $\pm 1.49 \mu\text{A cm}^{-2}$. (b_1) cathodic current; (b_2) anodic current. Depolarization is shown upward. Temperature 19°C . (c) Similar records from another fibre enlarged to have same time scale. Current strengths are $\pm 0.55 \mu\text{A cm}^{-2}$. Temperature 18°C . The response is unusually oscillatory.

Figs 21a and 24, but the action potentials are not plotted on a slow enough time base or with a large enough vertical scale to show the oscillations which follow the positive phase.

The corresponding oscillatory behaviour of the real nerve could be seen after a spike or a subthreshold short shock, but was best studied by passing a small constant current through the membrane and recording the changes of membrane potential that resulted. The current was supplied by the long internal electrode so that the whole area of membrane was subjected to a uniform current density. It was found that when the current was very weak the potential changes resulting from inward current (anodal) were almost exactly similar to those resulting from an equal outward current, but with opposite sign. This is shown in Figs 23b and c, where the potential changes are about $\pm 1 \text{ mV}$. This symmetry with weak currents is to be expected from our equations, since they can be reduced to a linear form when the displacements of all the variables from their resting values are small. Thus, neglecting products, squares and higher powers of δV , δm , δn and δh , the deviations of V , m , n and h

from their resting values (0 , m_0 , n_0 and h_0 respectively), equation (26) becomes:

$$\begin{aligned} \delta I = C_M \frac{d \delta V}{dt} + \bar{g}_K n_0^4 \delta V - 4\bar{g}_K n_0^3 V_K \delta n + \bar{g}_{Na} m_0^3 h_0 \delta V \\ - 3\bar{g}_{Na} m_0^2 h_0 V_{Na} \delta m - \bar{g}_{Na} m_0^3 V_{Na} \delta h + \bar{g}_1 \delta V. \end{aligned} \quad (35)$$

Similarly, equation (7) (p. 43; p. 518 of original paper) becomes:

$$\frac{d \delta n}{dt} = \frac{\partial \alpha_n}{\partial V} \delta V - (\alpha_n + \beta_n) \delta n - n_0 \frac{\partial (\alpha_n + \beta_n)}{\partial V} \delta V,$$

or:

$$(p + \alpha_n + \beta_n) \delta n = \left\{ \frac{\partial \alpha_n}{\partial V} - n_0 \frac{\partial (\alpha_n + \beta_n)}{\partial V} \right\} \delta V, \quad (36)$$

where p represents d/dt , the operation of differentiating with respect to time.

The quantity δn can be eliminated between equations (35) and (36). This process is repeated for δm and δh , yielding a fourth-order linear differential equation with constant coefficients for δV . This can be solved by standard methods for any particular time course of the applied current density δI .

Figure 23a shows the response of the membrane to a constant current pulse calculated in this way. The constants in the equations are chosen to be appropriate to a temperature of 18.5°C so as to make the result comparable with the tracings of experimental records shown in b and c. It will be seen that the calculated curve agrees well with the records in b, while those in c, obtained from another axon, are much less heavily damped and show a higher frequency of oscillation. A fair degree of variability is to be expected in these respects since both frequency and damping depend on the values of the components of the resting conductance. Of these, g_{Na} and g_K depend critically on the resting potential, while \bar{g}_1 is very variable from one fibre to another.

Both theory and experiment indicate a greater degree of oscillatory behaviour than is usually seen in a cephalopod nerve in a medium of normal ionic composition. We believe that this is largely a direct result of using the long internal electrode. If current is applied to a whole nerve through a point electrode, neighbouring points on the membrane will have different membrane potentials and the resulting currents in the axis cylinder will increase the damping.

The linear solution for the behaviour of the theoretical membrane at small displacements provide a convenient check on our step-by-step numerical procedure. The response of the membrane at 6.3°C to a small short shock was calculated by this means and compared with the step-by-step solution for an

initial depolarization of the membrane by 2 mV. The results are plotted in Fig. 24. The agreement is very close, the step-by-step solution deviating in the direction that would be expected to result from its finite amplitude (cf. Fig. 21).

As pointed out by Cole (1941), the process underlying oscillations in membrane potential must be closely connected with the inductive reactance observed with alternating currents. In our theoretical model the inductance is due partly to the inactivation process and partly to the change in potassium conductance, the latter being somewhat more important. For small displacements of the resting potential the variations in potassium current in 1 cm^2 of membrane are identical with those in a circuit containing a resistance of 820Ω in series with an inductance which is shunted by a resistance of 1900Ω . The value of the inductance is 0.39 H at 25°C , which is of the same order as the 0.2 H found by Cole and Baker (1941). The calculated inductance increases three-fold for a 10°C fall in temperature and decreases rapidly as the membrane potential is increased; it disappears at the potassium potential and is replaced by a capacity for $E > E_K$.

6. Discussion. The results presented here show that the equations derived in Section 2 of this paper predict with fair accuracy many of the electrical properties of the squid giant axon: the form, duration and amplitude of spike, both "membrane" and propagated; the conduction velocity; the impedance changes during the spike; the refractory period; ionic exchanges; subthreshold responses; and oscillations. In addition, they account at least qualitatively for many of the phenomena of excitation, including anode break excitation and accommodation. This is a satisfactory degree of agreement, since the equations and constants were derived entirely from "voltage clamp" records, without any adjustment to make them fit the phenomena to which they were subsequently applied. Indeed any such adjustment would be extremely difficult, because in most cases it is impossible to tell in advance what effect a given change in one of the equations will have on the final solution.

The agreement must not be taken as evidence that our equations are anything more than an empirical description of the time-course of the changes in permeability to sodium and potassium. An equally satisfactory description of the voltage clamp data could no doubt have been achieved with equations of very different form, which would probably have been equally successful in predicting the electrical behaviour of the membrane. It was pointed out in Section 2 of this paper that certain features of our equations were capable of a physical interpretation, but the success of the equations is no evidence in favour of the mechanism of permeability change that we tentatively had in mind when formulating them.

The point that we do consider to be established is that fairly simple permeability changes in response to alterations in membrane potential, of the

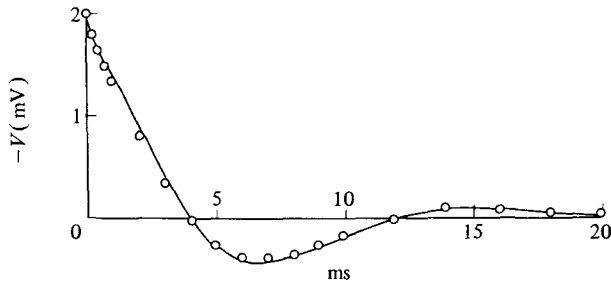


Figure 24. Comparison of step-by-step solution and linear approximation. Equation (26), temperature 6°C ; initial displacement of $-V=2\text{ mV}$. Continuous line: step-by-step solution. Circles: linear approximation with same initial displacement.

kind deduced from the voltage clamp results, are a sufficient explanation of the wide range of phenomena that have been fitted by solutions of the equations.

6.1. Range of applicability of the equations. The range of phenomena to which our equations are relevant is limited in two respects: in the first place, they cover only the short-term responses of the membrane, and in the second, they apply in their present form only to the isolated squid giant axon.

6.1.1. Slow changes. A nerve fibre whose membrane was described by our equations would run down gradually, since even in the resting state potassium leaves and sodium enters the axis cylinder, and both processes are accelerated by activity. This is no defect in describing the isolated squid giant axon, which does in fact run down in this way, but some additional process must take place in a nerve in the living animal to maintain the ionic gradients which are the immediate source of the energy used in impulse conduction.

6.1.2. After-potentials. Our equations give no account of after-potentials, apart from the positive phase and subsequent oscillations.

6.1.3. Conditions of isolated giant axon. There are many reasons for supposing that the resting potential of the squid giant axon is considerably lower after isolation than when it is intact in the living animal. Further evidence for this view is provided by the observation (Hodgkin and Huxley, 1952c) that the maximum inward current that the membrane can pass on depolarization is increased by previously raising the resting potential by 10–20 mV by means of anodally directed current. Our equations could easily be modified to increase the resting potential (e.g. by reducing the leak conductance and adding a small outward current representing metabolic extrusion of sodium ions). We have not made any calculations for such a case, but certain qualitative results are

evident from inspection of other solutions. If, for instance, the resting potential were raised (by 12 mV) to the potassium potential, the positive phase and subsequent oscillations after the spike would disappear, the rate of rise of the spike would be increased, the exchange of internal and external sodium in a spike would be increased, the membrane would not be oscillatory unless depolarized, and accommodation and the tendency to give anode break responses would be greatly reduced. Several of these phenomena have been observed when the resting potential of frog nerve is raised (Lorente de Nó, 1947), but no corresponding information exists about the squid giant axon.

6.1.4. *Applicability to other tissues.* The similarity of the effects of changing the concentrations of sodium and potassium on the resting and action potentials of many excitable tissues (Hodgkin, 1951) suggests that the basic mechanism of conduction may be the same as implied by our equations, but the great differences in the shape of action potentials show that even if equations of the same form as ours are applicable in other cases, some at least of the parameters must have very different values.

6.2. *Differences between calculated and observed behaviour.* In the Results section, a number of points were noted on which the calculated behaviour of our model did not agree with the experimental results. We shall now discuss the extent to which these discrepancies can be attributed to known shortcomings in our equations. Two such shortcomings were pointed out in Section 2 of this paper, and were accepted for the sake of keeping the equations simple. One was that the membrane capacity was assumed to behave as a "perfect" condenser (phase angle 90° ; p. 30; p. 505 of original paper), and the other was that the equations governing the potassium conductance do not give as much delay in the conductance rise on depolarization (e.g. to the sodium potential) as was observed in voltage clamps (pp. 34–35; p. 509 of original paper).

The assumption of a perfect capacity probably accounts for the fact that the initial fall in potential after application of a short shock is much less marked in the calculated than in the experimental curves (Figs 12 and 21). Some of the initial drop in the experimental curves may also be due to end-effects, the guard system being designed for the voltage clamp procedure but not for stimulation by short shocks.

The inadequacy of the delay in the rise of potassium conductance has several effects. In the first place the falling phase of the spike develops too early, reducing the spike amplitude slightly and making the peak too pointed in shape (pp. 51–52; p. 525 of original paper). In the membrane action potentials these effects become more marked the smaller the stimulus, since the potassium conductance begins to rise during the latent period. This causes the spike amplitude to decrease more in the calculated than in the experimental curves (Fig. 12).

The low calculated value for the exchange of internal and external sodium ions is probably due to this cause. Most of the sodium exchange occurs near the peak of the spike, when the potential is close to the sodium potential. The early rise of potassium conductance prevents the potential from getting as close to the sodium potential, and from staying there for as long a time, as it should.

A check on these points is provided by the "anode break" action potential. Until the break of the applied current, the quantity n has the steady-state value appropriate to $V = +30$ mV, i.e. it is much smaller than in the usual resting condition. This greatly increases the delay in the rise of potassium conductance when the membrane is depolarized. It was found that the spike height was greater (Table 4), the peak was more rounded, and the exchange of internal and external sodium was greater (Table 5), than in an action potential which followed a cathodal short shock.

The other important respect in which the model results disagreed with the experimental was that the calculated exchange of internal and external potassium ions per impulse was too large. This exchange took place largely during the positive phase, when the potential is close to the potassium potential and the potassium conductance is still fairly high. We have no satisfactory explanation for this discrepancy, but it is probably connected with the fact that the value of the potassium potential was less strongly affected by changes in external potassium concentration than is required by the Nernst equation.

7. Summary

- (1) The voltage clamp data obtained previously are used to find equations which describe the changes in sodium and potassium conductance associated with an alteration of membrane potential. The parameters in these equations were determined by fitting solutions to the experimental curves relating sodium or potassium conductance to time at various membrane potentials.
- (2) The equations, given on pp. 43–44; pp. 518–519 of original paper, were used to predict the quantitative behaviour of a model nerve under a variety of conditions which corresponded to those in actual experiments. Good agreement was obtained in the following cases: (a) the form, amplitude and threshold of an action potential under zero membrane current at two temperatures; (b) the form, amplitude and velocity of a propagated action potential; (c) the form and amplitude of the impedance changes associated with an action potential; (d) the total inward movement of sodium ions and the total outward movement of potassium ions associated with an impulse; (e) the threshold and response during the refractory period; (f) the existence and form of subthreshold responses; (g) the existence and form of an anode break response; (h) the properties of the subthreshold oscillations seen in cephalopod axons.

- (3) The theory also predicts that a direct current will not excite if it rises sufficiently slowly.
- (4) Of the minor defects the only one for which there is no fairly simple explanation is that the calculated exchange of potassium ions is higher than that found in *Sepia* axons.
- (5) It is concluded that the responses of an isolated giant axon of *Loligo* to electrical stimuli are due to reversible alterations in sodium and potassium permeability arising from changes in membrane potential.

LITERATURE

- Cole, K. S. 1941. Rectification and inductance in the squid giant axon. *J. gen. Physiol.* **25**, 29–51.
- Cole, K. S. and R. F. Baker. 1941. Longitudinal impedance of the squid giant axon. *J. gen. Physiol.* **24**, 771–788.
- Cole, K. S. and H. J. Curtis. 1939. Electric impedance of the squid giant axon during activity. *J. gen. Physiol.* **22**, 649–670.
- Goldman, D. E. 1943. Potential, impedance and rectification in membranes. *J. gen. Physiol.* **27**, 37–60.
- Hartree, D. R. 1932/3. A practical method for the numerical solution of differential equations. *Mem. Manch. lit. phil. Soc.* **77**, 91–107.
- Hodgkin, A. L. 1951. The ionic basis of electrical activity in nerve and muscle. *Biol. Rev.* **26**, 339–409.
- Hodgkin, A. L. and A. F. Huxley. 1952a. Currents carried by sodium and potassium ions through the membrane of the giant axon of *Loligo*. *J. Physiol.* **116**, 449–472.
- Hodgkin, A. L. and A. F. Huxley. 1952b. The components of membrane conductance in the giant axon of *Loligo*. *J. Physiol.* **116**, 473–496.
- Hodgkin, A. L. and A. F. Huxley. 1952c. The dual effect of membrane potential on sodium conductance in the giant axon of *Loligo*. *J. Physiol.* **116**, 497–506.
- Hodgkin, A. L., A. F. Huxley, and B. Katz. 1949. Ionic currents underlying activity in the giant axon of the squid. *Arch. Sci. physiol.* **3**, 129–150.
- Hodgkin, A. L., A. F. Huxley and B. Katz. 1952. Measurement of current–voltage relations in the membrane of the giant axon of *Loligo*. *J. Physiol.* **116**, 424–448.
- Hodgkin, A. L. and B. Katz. 1949. The effect of temperature on the electrical activity of the giant axon of the squid. *J. Physiol.* **109**, 240–249.
- Keynes, R. D. 1951. The ionic movements during nervous activity. *J. Physiol.* **114**, 119–150.
- Keynes, R. D. and P. R. Lewis. 1951. The sodium and potassium content of cephalopod nerve fibres. *J. Physiol.* **114**, 151–182.
- Lorente de Nó, R. 1947. A study of nerve physiology. *Stud. Rockefeller Inst. med. Res.* **131**, 132.
- Pumphrey, R. J., O. H. Schmitt and J. Z. Young. 1940. Correlation of local excitability with local physiological response in the giant axon of the squid (*Loligo*). *J. Physiol.* **98**, 47–72.